Chapter 4
Dynamics and Control of a Gyroscope

In this chapter theoretical investigations and the results of computer simulations are presented to show that the following factors affect the accuracy of realization of the required motion of a controlled gyroscope axis:

1. Compliance of initial conditions of the gyroscope motion with imposed initial conditions. In order to guide the gyroscope axis to the appropriate initial position one can apply additional time-independent control.
2. Values of the resistant-force coefficients in the bearings of gyroscope frames. Too small values of these coefficients, during external disturbance or kinematic excitation of the base, cause dynamical effects to arise and decrease the accuracy of realization of the preset motion. However, large values make the gyroscope axis drift off the preset position in space. Thus, one needs to minimalize the friction coefficients in the bearings of the gyroscope suspension and, additionally, to apply optimally selected dampers.
3. Influence of non-linearities in the model of gyroscope motion, which manifests especially at large angular deviations of the gyroscope axis.
4. Additional deviations of gyroscope—which, independently of the numerous technological tricks, always emerge during gyroscope operation—need to be reduced by means of the gyroscope's automatic control system. The proper position of the gyroscope axis is maintained by the automatic control system on the basis of the real position obtained from measurements and the required position of the gyroscope axis worked out by a digital machine.

4.1 Dynamics of a Gyroscope on a Movable Platform

Figure 4.1 shows a general view of a gyroscope and a movable base [board of flying object (FO)] along with acting forces and torques. We introduce the following frames [1–3]: $O_{g1}X_1'X_2'X_3'$—movable frame fixed to an external frame

J. Awrejcewicz and Z. Koruba, *Classical Mechanics*, Advances in Mechanics and Mathematics 30, DOI 10.1007/978-1-4614-3978-3_4,

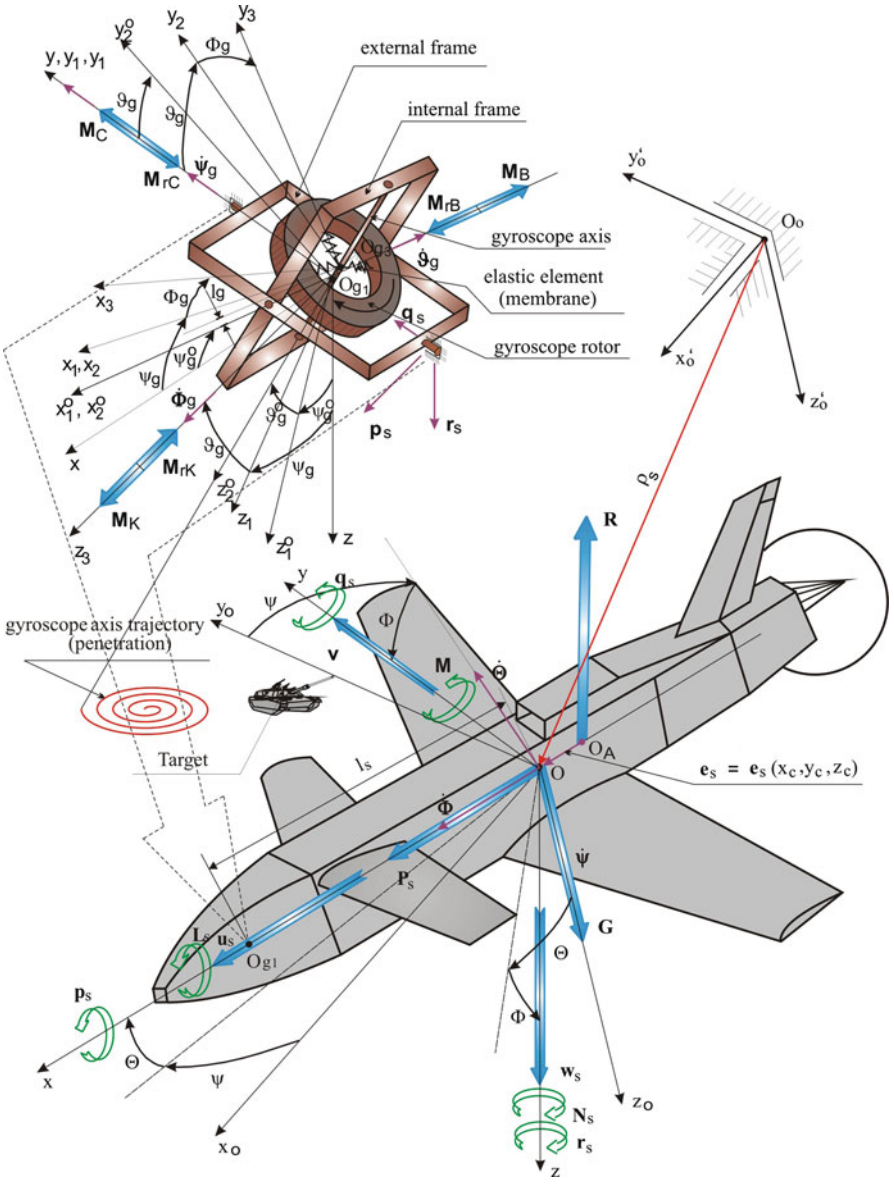

Fig. 4.1 General view of a gyroscope placed on a movable base (board of FO)

of the gyroscope; $O_{g_2}X_1''X_2''X_3''$—movable frame fixed to an internal frame of the gyroscope; $O_{g_3}X_1'''X_2'''X_3'''$—movable frame fixed to a rotor of the gyroscope; $O_{g_2}X_{10}''X_{20}''X_{30}''$—movable frame fixed to an axis of the gyroscope.

The mutual angular position of axes of the frames will be determined by means of a transformation matrix in the following way. The transformation matrix from the frame fixed to the platform to the frame fixed to the external frame governing the rotation of the frame $O_{g_1}X_1'X_2'X_3'$ relative to $OX_1X_2X_3$ about the axis $O_{g_1}X_2'$ at angle ψ_g has the following form:

$$M_{pz} = \begin{bmatrix} \cos\psi_g & 0 & -\sin\psi_g \\ 0 & 1 & 0 \\ \sin\psi_g & 0 & \cos\psi_g \end{bmatrix}. \tag{4.1}$$

The transformation matrix from the frame fixed to the external frame to that fixed to the internal frame (rotation of the frame $O_{g_2}X_1''X_2''X_3''$ relative to $O_{g_1}X_1'X_2'X_3'$ about the axis $O_{g_2}X_1''$ at angle ϑ_g) is as follows:

$$M_{zw} = \begin{bmatrix} 1 & 0 & 0 \\ 0 & \cos\vartheta_g & \sin\vartheta_g \\ 0 & -\sin\vartheta_g & \cos\vartheta_g \end{bmatrix}. \tag{4.2}$$

The transformation matrix from the frame fixed to the internal frame to that fixed to the rotor (rotation of the frame $O_{g_3}X_1'''X_2'''X_3'''$ relative to $O_{g_2}X_1''X_2''X_3''$ about the axis $O_{g_3}X_3'''$ at angle Φ_g) reads

$$M_{wr} = \begin{bmatrix} \cos\Phi_g & \sin\Phi_g & 0 \\ -\sin\Phi_g & \cos\Phi_g & 0 \\ 0 & 0 & 1 \end{bmatrix}. \tag{4.3}$$

The transformation matrix from the frame fixed to the platform to that fixed to the internal frame is obtained in the following way:

$$M_{pw} = M_{zw} \cdot M_{pz} = \begin{bmatrix} \cos\psi_g & 0 & -\sin\psi_g \\ \sin\vartheta_g \sin\psi_g & \cos\vartheta_g & \sin\vartheta_g \cos\psi_g \\ \cos\vartheta_g \sin\psi_g & -\sin\vartheta_g & \cos\vartheta_g \cos\psi_g \end{bmatrix}, \tag{4.4}$$

and the transformation matrix from the frame fixed to the platform to that fixed to the rotor is as follows:

$$M_{pr} = M_{wr} \cdot M_{pw} = \begin{bmatrix} \cos\psi_g \cos\Phi_g + & & -\sin\psi_g \cos\Phi_g \\ +\sin\vartheta_g \sin\psi_g \sin\Phi_g & \cos\vartheta_g \sin\Phi_g & +\sin\vartheta_g \cos\psi_g \sin\Phi_g \\ -\cos\psi_g \sin\Phi_g + & & \sin\psi_g \cos\Phi_g + \\ +\sin\vartheta_g \sin\psi_g \cos\Phi_g & \cos\vartheta_g \cos\Phi_g & +\sin\vartheta_g \cos\psi_g \sin\Phi_g \\ \cos\vartheta_g \sin\psi_g & -\sin\vartheta_g & \cos\vartheta_g \cos\psi_g \end{bmatrix}. \tag{4.5}$$

In the case where the gyroscope axis is connected with the rotor by means of an elastic element, the gyroscope gains an additional two degrees of freedom, and the corresponding matrices of transformation (analogically M_{pz}, M_{zw} and M_{pw}) take

the form

$$M_{pz}^{0} = \begin{bmatrix} \cos\psi_g^0 & 0 & -\sin\psi_g^0 \\ 0 & 1 & 0 \\ \sin\psi_g^0 & 0 & \cos\psi_g^0 \end{bmatrix},$$

$$M_{zw}^{0} = \begin{bmatrix} 1 & 0 & 0 \\ 0 & \cos\vartheta_g^0 & \sin\vartheta_g^0 \\ 0 & -\sin\vartheta_g^0 & \cos\vartheta_g^0 \end{bmatrix},$$

$$M_{pw}^{0} = M_{pz}^{0} \cdot M_{zw}^{0} = \begin{bmatrix} \cos\psi_g^0 & 0 & -\sin\psi_g^0 \\ \sin\vartheta_g^0\sin\psi_g^0 & \cos\vartheta_g^0 & \sin\vartheta_g^0\cos\psi_g^0 \\ \cos\vartheta_g^0\sin\psi_g^0 & -\sin\vartheta_g^0 & \cos\vartheta_g^0\cos\psi_g^0 \end{bmatrix}. \tag{4.6}$$

The following assumptions are introduced:

1. The center of mass of the rotor coincides with the center of mass of the internal frame $O_{g_2} = O_{g_3}$, but it does not coincide with the center of motion O_{g_1}, i.e., with the point of intersection of the axes of rotor rotation and the frames. Hence, we consider a non-astatic gyroscope, also called a "heavy" gyroscope.
2. The axes $O_{g_1}X_1'$, $O_{g_1}X_2'$, $O_{g_1}X_3'$ are the main, central axes of inertia of the external frame; similarly, the axes $O_{g_2}X_3''$ and $O_{g_3}X_3'''$ are the main, central axes of inertia of the internal frame and the rotor, respectively. The remaining axes are the main ones of the corresponding systems.

The given quantities follow:

1. m_1, m_2, m_3—masses of external frame, internal (along with the axis) frame, and rotor of gyroscope, respectively.
2. l_s—distance between center of mass of base and center of gyroscope motion.
3. l_g—distance between center of mass of system: rotor—internal frame and center of motion.
4. $I_{X_1'}, I_{X_2'}, I_{X_3'}$—moments of inertia of external frame about axes $O_{g_1}X_1'$, $O_{g_1}X_2'$, $O_{g_1}X_3'$, respectively.
5. $I_{X_1''}, I_{X_2''}, I_{X_3''}$—moments of inertia of internal frame about axes $O_{g_2}X_1''$, $O_{g_2}X_2''$, $O_{g_2}X_3''$, respectively.
6. $I_{X_1'''}, I_{X_2'''}, I_{X_3'''}$—moments of inertia of rotor about axes $O_{g_3}X_1'''$, $O_{g_3}X_2'''$, $O_{g_3}X_3'''$, respectively.
7. $I^0_{X_1''}, I^0_{X_2''}$—moments of inertia of gyroscope axis about axes $O_{g_2}X_{10}''$, $O_{g_2}X_{20}''$, respectively.
8. $\boldsymbol{\omega}_g(p^*, q^*, r^*)$—components of angular velocity vector of base (kinematic interaction of the base).
9. $\mathbf{V}_g^*(V_{gX_1}, V_{gX_2}, V_{gX_3})$—components of linear velocity vector of base displacement—coordinates of point O_{g_1}.

10. $\mathbf{F}_g(F_{gX_1}, F_{gX_2}, F_{gX_3})$—components of force acting on center of mass of rotor in frame fixed to platform $O_{g_1}X_1X_2X_3$.
11. Moments of forces of interactions:
    (a) $\mathbf{M}_c(M_{cX_1}, M_{cX_2}, M_{cX_3})$—base on external frame;
    (b) $\mathbf{M}_b(M_{bX_1'}, M_{bX_2'}, M_{bX_3'})$—external frame on internal one;
    (c) $\mathbf{M}_k(M_{kX_1''}, M_{kX_2''}, M_{kX_3''})$—internal frame on rotor.
12. Moments of friction forces in bearings of internal and external frames:
    (a) Viscous

$$M_{rc} = M_{rc}^V = \eta_c \frac{\mathrm{d}\psi_g}{\mathrm{d}t}, \quad M_{rb} = M_{rb}^V = \eta_b \frac{\mathrm{d}\vartheta_g}{\mathrm{d}t};$$

    (b) Dry

$$M_{rc} = M_{rc}^{\mathrm{T}} = 0,5 \cdot T_{rc} \cdot d_c, \quad M_{rb} = M_{rb}^{\mathrm{T}} = 0,5 \cdot T_{rb} \cdot d_b;$$

    where

$$T_{rc} = \mu_c N_c sign\Big(\frac{\mathrm{d}\psi_g}{\mathrm{d}t}\Big), \qquad T_{rb} = \mu_b N_b sign\Big(\frac{\mathrm{d}\vartheta_g}{\mathrm{d}t}\Big),$$

    and $\eta_c, \eta_b, \mu_c, \mu_b$ are friction coefficients in the frame bearings; N_c, N_b are normal reactions in the bearings; d_c, d_b are diameters of the bearing pins.
13. M_{rk}—moment of friction forces in bearing of rotor in internal frame and aerodynamic resistance.
14. M_{zb}, M_{zc}—disturbing signals in form of torques acting directly on rotor.
15. κ—stiffness coefficient of elastic element connecting axis with rotor.

The desired quantities are as follows:

1. $\psi_g, \vartheta_g, \Phi_g$—angles by means of which one determines the position of the rotor relative to the frame $O_{g_1}X_1X_2X_3$;
2. ψ_g^0, ϑ_g^0—angles by means of which one determines the position of the gyroscope axis relative to the frame $O_{g_1}X_1X_2X_3$;
3. Angular velocities: $\dot{\psi}_g = \frac{\mathrm{d}\psi_g}{\mathrm{d}t}, \quad \dot{\vartheta}_g = \frac{\mathrm{d}\vartheta_g}{\mathrm{d}t}, \quad \dot{\Phi}_g = \frac{\mathrm{d}\Phi_g}{\mathrm{d}t}$;
4. Angular velocities: $\dot{\psi}_g^0 = \frac{\mathrm{d}\psi_g^0}{\mathrm{d}t}, \quad \dot{\vartheta}_g^0 = \frac{\mathrm{d}\vartheta_g^0}{\mathrm{d}t}, \quad \dot{\Phi}_g^0 = \frac{\mathrm{d}\Phi_g^0}{\mathrm{d}t}$.

The vector of the angular velocity of the rotor reads

$$\boldsymbol{\omega}_g^* = \frac{d\boldsymbol{\psi}_g}{\mathrm{d}t} + \frac{d\boldsymbol{\vartheta}_g}{\mathrm{d}t} + \frac{d\boldsymbol{\Phi}_g}{\mathrm{d}t}, \tag{4.7}$$

whereas the angular velocity vector of the gyroscope has the following form:

$$\boldsymbol{\omega}_g^0 = \frac{d\boldsymbol{\psi}_g^0}{\mathrm{d}t} + \frac{d\boldsymbol{\vartheta}_g^0}{\mathrm{d}t}. \tag{4.8}$$

Projections of its components on particular axes of the coordinate system can be determined as follows:

$$\begin{bmatrix} \dot{\psi}_{gX_1'} \\ \dot{\psi}_{gX_2'} \\ \dot{\psi}_{gX_3'} \end{bmatrix} = \begin{bmatrix} 0 \\ \dot{\psi}_g \\ 0 \end{bmatrix}, \qquad \begin{bmatrix} \dot{\psi}_{gX_1''} \\ \dot{\psi}_{gX_2''} \\ \dot{\psi}_{gX_3''} \end{bmatrix} = \begin{bmatrix} 0 \\ \dot{\psi}_g \cos\vartheta_g \\ -\dot{\psi}_g \sin\vartheta_g \end{bmatrix},$$

$$\begin{bmatrix} \dot{\psi}_{gX_1'''} \\ \dot{\psi}_{gX_2'''} \\ \dot{\psi}_{gX_3'''} \end{bmatrix} = \begin{bmatrix} \dot{\psi}_g \cos\vartheta_g \sin\Phi_g \\ \dot{\psi}_g \cos\vartheta_g \cos\Phi_g \\ -\dot{\psi}_g \sin\vartheta_g \end{bmatrix}, \tag{4.9}$$

$$\begin{bmatrix} \dot{\vartheta}_{gX_1'} \\ \dot{\vartheta}_{gX_2'} \\ \dot{\vartheta}_{gX_3'} \end{bmatrix} = \begin{bmatrix} \dot{\vartheta}_g \cos\psi_g \\ 0 \\ -\dot{\vartheta}_g \sin\psi_g \end{bmatrix}, \qquad \begin{bmatrix} \dot{\vartheta}_{gX_1''} \\ \dot{\vartheta}_{gX_2''} \\ \dot{\vartheta}_{gX_3''} \end{bmatrix} = \begin{bmatrix} \dot{\vartheta}_g \\ 0 \\ 0 \end{bmatrix},$$

$$\begin{bmatrix} \dot{\vartheta}_{gX_1'''} \\ \dot{\vartheta}_{gX_2'''} \\ \dot{\vartheta}_{gX_3'''} \end{bmatrix} = \begin{bmatrix} \dot{\vartheta}_g \cos\Phi_g \sin \\ -\dot{\vartheta}_g \sin\Phi_g \\ 0 \end{bmatrix}, \qquad \begin{bmatrix} \dot{\Phi}_{gX_1'''} \\ \dot{\Phi}_{gX_2'''} \\ \dot{\Phi}_{gX_3'''} \end{bmatrix} = \begin{bmatrix} 0 \\ 0 \\ \dot{\Phi}_g \end{bmatrix}. \tag{4.10}$$

Analogously, projections of the components of the angular velocity vector of the gyroscope axis will take the following forms:

$$\begin{bmatrix} \dot{\psi}^0_{gX_1'} \\ \dot{\psi}^0_{gX_2'} \\ \dot{\psi}^0_{gX_3'} \end{bmatrix} = \begin{bmatrix} 0 \\ \dot{\psi}^0_g \\ 0 \end{bmatrix}, \qquad \begin{bmatrix} \dot{\psi}^0_{gX_1''} \\ \dot{\psi}^0_{gX_2''} \\ \dot{\psi}^0_{gX_3''} \end{bmatrix} = \begin{bmatrix} 0 \\ \dot{\psi}^0_g \cos\vartheta^0_g \\ -\dot{\psi}^0_g \sin\vartheta^0_g \end{bmatrix}, \tag{4.11}$$

$$\begin{bmatrix} \dot{\vartheta}^0_{gX_1'} \\ \dot{\vartheta}^0_{gX_2'} \\ \dot{\vartheta}^0_{gX_3'} \end{bmatrix} = \begin{bmatrix} \dot{\vartheta}^0_g \cos\psi^0_g \\ 0 \\ -\dot{\vartheta}^0_g \sin\psi^0_g \end{bmatrix}, \qquad \begin{bmatrix} \dot{\vartheta}^0_{gX_1''} \\ \dot{\vartheta}^0_{gX_2''} \\ \dot{\vartheta}^0_{gX_3''} \end{bmatrix} = \begin{bmatrix} \dot{\vartheta}^0_g \\ 0 \\ 0 \end{bmatrix}. \tag{4.12}$$

In what follows one may define the components of the angular velocity vector of the external frame in the coordinate system $O_{g_1}X_1'X_2'X_3'$:

$$\begin{bmatrix} \omega_{gX_1'} \\ \omega_{gX_2'} \\ \omega_{gX_3'} \end{bmatrix} = M_{pz} \begin{bmatrix} p^* \\ q^* \\ r^* \end{bmatrix} + \begin{bmatrix} \dot{\psi}_{gX_1'} \\ \dot{\psi}_{gX_2'} \\ \dot{\psi}_{gX_3'} \end{bmatrix} = \begin{bmatrix} p^* \cos\psi_g - r^* \sin\psi_g \\ \dot{\psi}_g + q^* \\ p^* \sin\psi_g + r^* \cos\psi_g \end{bmatrix}. \tag{4.13}$$

On the other hand, the components of the angular velocity vector of the internal frame in the coordinate system $O_{g_2}X_1''X_2''X_3''$ read

$$\begin{bmatrix} \omega_{gX_1''} \\ \omega_{gX_2''} \\ \omega_{gX_3''} \end{bmatrix} = M_{pw} \begin{bmatrix} p^* \\ q^* \\ r^* \end{bmatrix} + \begin{bmatrix} \dot{\vartheta}_{gX_1''} \\ \dot{\vartheta}_{gX_2''} \\ \dot{\vartheta}_{gX_3''} \end{bmatrix} + \begin{bmatrix} \dot{\psi}_{gX_1''} \\ \dot{\psi}_{gX_2''} \\ \dot{\psi}_{gX_3''} \end{bmatrix}$$

$$= \begin{bmatrix} p^* \cos\psi_g - r^* \sin\psi_g + \dot{\vartheta}_g \\ (p^* \sin\psi_g + r^* \cos\psi_g)\sin\vartheta_g + (q^* + \dot{\psi}_g)\cos\vartheta_g \\ (p^* \sin\psi_g + r^* \cos\psi_g)\cos\vartheta_g - (q^* + \dot{\psi}_g)\sin\vartheta_g \end{bmatrix}. \quad (4.14)$$

Components of the angular velocity vector in the coordinate system $O_{g_3}X_1'''X_2'''X_3'''$ have the form

$$\begin{bmatrix} \omega_{gX_1'''} \\ \omega_{gX_2'''} \\ \omega_{gX_3'''} \end{bmatrix} = M_{pr} \begin{bmatrix} p^* \\ q^* \\ r^* \end{bmatrix} + \begin{bmatrix} \dot{\vartheta}_{gX_1'''} \\ \dot{\vartheta}_{gX_2'''} \\ \dot{\vartheta}_{gX_3'''} \end{bmatrix} + \begin{bmatrix} \dot{\psi}_{gX_1'''} \\ \dot{\psi}_{gX_2'''} \\ \dot{\psi}_{gX_3'''} \end{bmatrix} + \begin{bmatrix} \dot{\Phi}_{gX_1'''} \\ \dot{\Phi}_{gX_2'''} \\ \dot{\Phi}_{gX_3'''} \end{bmatrix},$$

or, equivalently,

$$\begin{aligned} \omega_{gX_1'''} &= p^*(\cos\psi_g \cos\Phi_g + \sin\vartheta_g \sin\psi_g \sin\Phi_g) \\ &\quad + (q^* + \dot{\psi}_g)\cos\vartheta_g \sin\Phi_g + \dot{\vartheta}_g \cos\Phi_g \\ &\quad + r^*(\cos\psi_g \sin\vartheta_g \sin\Phi_g - \sin\psi_g \cos\Phi_g), \quad (4.15) \\ \omega_{gX_2'''} &= -p^*(\cos\psi_g \sin\Phi_g - \sin\vartheta_g \sin\psi_g \cos\Phi_g) \\ &\quad + (q^* + \dot{\psi}_g)\cos\vartheta_g \cos\Phi_g - \dot{\vartheta}_g \sin\Phi_g \\ &\quad + r^*(\cos\psi_g \sin\vartheta_g \cos\Phi_g + \sin\psi_g \sin\Phi_g), \quad (4.16) \\ \omega_{gX_3'''} &= p^* \sin\psi_g \cos\vartheta_g - (q^* + \dot{\psi}_g)\sin\vartheta_g \\ &\quad + r^* \cos\psi_g \cos\vartheta_g + \dot{\Phi}_g. \quad (4.17) \end{aligned}$$

Components of the velocity vector of the gyroscope axis in the coordinate system $O_{g_1}X_1'X_2'X_3'$ read

$$\begin{bmatrix} \omega^0_{gX_1'} \\ \omega^0_{gX_2'} \\ \omega^0_{gX_3'} \end{bmatrix} = M^0_{pz} \begin{bmatrix} p^* \\ q^* \\ r^* \end{bmatrix} + \begin{bmatrix} \dot{\psi}^0_{gX_1'} \\ \dot{\psi}^0_{gX_2'} \\ \dot{\psi}^0_{gX_3'} \end{bmatrix} = \begin{bmatrix} p^* \cos\psi^0_g - r^* \sin\psi^0_g \\ \dot{\psi}^0_g + q^* \\ p^* \sin\psi^0_g + r^* \cos\psi^0_g \end{bmatrix}. \quad (4.18)$$

Finally, components of the velocity vector of the gyroscope axis in the coordinate system $O_{g_2}X''_{10}X''_{20}X''_{30}$ are as follows:

$$\begin{bmatrix} \omega^0_{gX''_1} \\ \omega^0_{gX''_2} \\ \omega^0_{gX''_3} \end{bmatrix} = M_{pw} \begin{bmatrix} p^* \\ q^* \\ r^* \end{bmatrix} + \begin{bmatrix} \dot{\vartheta}^0_{gX''_1} \\ \dot{\vartheta}^0_{gX''_2} \\ \dot{\vartheta}^0_{gX''_3} \end{bmatrix} + \begin{bmatrix} \dot{\psi}^0_{gX''_1} \\ \dot{\psi}^0_{gX''_2} \\ \dot{\psi}^0_{gX''_3} \end{bmatrix}$$

$$= \begin{bmatrix} p^* \cos\psi^0_g - r^* \sin\psi^0_g + \dot{\vartheta}^0_g \\ (p^* \sin\psi^0_g + r^* \cos\psi^0_g) \sin\vartheta^0_g + (q^* + \dot{\psi}^0_g) \cos\vartheta^0_g \\ (p^* \sin\psi^0_g + r^* \cos\psi^0_g) \cos\vartheta^0_g - (q^* + \dot{\psi}^0_g) \sin\vartheta^0_g \end{bmatrix}. \quad (4.19)$$

The linear velocity of the center of mass of the rotor is a sum of the drift velocity of point O_s (velocity of FO) and O_{g_1} (about point O_s) and the relative velocity relative to point O_{g_2} [2,4]:

$$\mathbf{V}_{g_2} = \mathbf{V}_s + \begin{vmatrix} \mathbf{E}_1 & \mathbf{E}_2 & \mathbf{E}_3 \\ \mathbf{p}^* & \mathbf{q}^* & \mathbf{r}^* \\ l_s & 0 & 0 \end{vmatrix} + \begin{vmatrix} \mathbf{E}'_1 & \mathbf{E}'_2 & \mathbf{E}'_3 \\ \omega_{gX'_1} & \omega_{gX'_2} & \omega_{gX'_3} \\ 0 & 0 & l_g \end{vmatrix} + \begin{vmatrix} \mathbf{E}''_1 & \mathbf{E}''_2 & \mathbf{E}''_3 \\ \omega_{gX''_1} & \omega_{gX''_2} & \omega_{gX''_3} \\ 0 & 0 & l_g \end{vmatrix},$$

or, equivalently,

$$V_{gX''_1} = u_s \cos\psi_g - (w_s - q^* l_s) \sin\psi_g + (\omega_{gX'_2} + \omega_{gX''_2}) l_g, \quad (4.20)$$

$$V_{gX''_2} = (u_s \sin\psi_g + (w_s - q^* l_s) \cos\psi_g) \sin\vartheta_g + (v_s + r^* l_s) \cos\vartheta_g - (\omega_{gX''_1} + \omega_{gX'_1} \cos\vartheta_g) l_g, \quad (4.21)$$

$$V_{gX''_3} = (u_s \sin\psi_g + (w_s - q^* l_s) \cos\psi_g) \cos\vartheta_g - (v_s + r^* l_s) \sin\vartheta_g + \omega_{gX'_1} l_g \sin\vartheta_g. \quad (4.22)$$

The linear velocity of the center of mass of the external frame reads

$$\mathbf{V}_{g_1} = \mathbf{V}_s + \begin{vmatrix} \mathbf{E}_1 & \mathbf{E}_2 & \mathbf{E}_3 \\ \mathbf{p}^* & \mathbf{q}^* & \mathbf{r}^* \\ l_s & 0 & 0 \end{vmatrix},$$

or, equivalently,

$$V_{gX'_1} = u_s \cos\psi_g - (w_s - q^* l_s) \sin\psi_g, \quad (4.23)$$

$$V_{gX'_2} = v_s + r^* l_s, \quad (4.24)$$

$$V_{gX'_3} = u_s \sin\psi_g + (w_s - q^* l_s) \cos\psi_g. \quad (4.25)$$

Similarly, projections of the linear velocity of the center of mass of the external frame-axis system are

$$V^0_{gX''_1} = u_s \cos\psi^0_g - (w_s - q^* l_s)\sin\psi^0_g + (\omega^0_{gX'_2} + \omega^0_{gX''_2}) l_g, \tag{4.26}$$

$$\begin{aligned} V^0_{gX''_2} = {} & (u_s \sin\psi^0_g + (w_s - q^* l_s)\cos\psi^0_g)\sin\vartheta^0_g \\ & + (v_s + r^* l_s)\cos\vartheta^0_g - (\omega^0_{gX''_1} + \omega^0_{gX'_1}\cos\vartheta^0_g) l_g, \end{aligned} \tag{4.27}$$

$$\begin{aligned} V^0_{gX''_3} = {} & (u_s \sin\psi^0_g + (w_s - q^* l_s)\cos\psi^0_g)\cos\vartheta^0_g \\ & - (v_s + r^* l_s)\sin\vartheta^0_g + \omega^0_{gX'_1} l_g \sin\vartheta^0_g. \end{aligned} \tag{4.28}$$

The axes $O_{g_1}X'_1$, $O_{g_1}X'_2$, $O_{g_1}X'_3$, $O_{g_2}X''_3$, and $O_{g_3}X'''_3$ are the main central axes of inertia of the corresponding frames. The remaining axes are the main ones of the suitable systems. By $I^*_{X''_1}$, $I^*_{X''_2}$, $I^*_{X''_3}$, $I^*_{X'''_1}$, $I^*_{X'''_2}$, and $I^*_{X'''_3}$ we denote the moments of inertia of the corresponding frames about the axes parallel to the axes $O_{g_2}X''_1$, $O_{g_2}X''_2$, $O_{g_2}X''_3$, $O_{g_3}X'''_1$, $O_{g_3}X'''_2$, and $O_{g_3}X'''_3$ but passing through the center of mass.

We will derive equations of motion of the gyroscope by means of the Lagrange equations of the second kind. To that end, we will determine the kinetic E_k (equal to the sum of the kinetic energy of the external and internal frames, the rotor, and the axis) and the potential E_p energy of the system

$$\begin{aligned} E_k = {} & \frac{1}{2}\big[I_{X'_1}\omega^2_{gX'} + I_{X'_2}\omega^2_{gX'_2} + I_{X'_3}\omega^2_{gX'_3}\big] \\ & + \frac{1}{2}\big[I^*_{X''_1}\omega^2_{gX''_1} + I^*_{X''_2}\omega^2_{gX''_2} + I^*_{X''_3}\omega^2_{gX''_3}\big] \\ & + \frac{1}{2}\big[I^*_{X'''_1}\omega^2_{gX'''_1} + I^*_{X'''_2}\omega^2_{gX'''_2} + I^*_{X'''_3}\omega^2_{gX'''_3}\big] \\ & + \frac{1}{2}\big[I^0_{X''_1}(\omega^0_{gX''_1})^2 + I^0_{X''_2}(\omega^0_{gX''_2})^2\big] \\ & + \frac{1}{2}m_3 V_s^2 + \frac{1}{2}m_1\big(V^2_{gX'} + V^2_{gX'_2} + V^2_{gX'_3}\big) \\ & + \frac{1}{2}m_3\big(V^2_{gX''_1} + V^2_{gX''_2} + V^2_{gX''_3}\big) \\ & + \frac{1}{2}m_2\big[(V^0_{gX''_1})^2 + (V^0_{gX''_2})^2 + (V^0_{gX''_3})^2\big], \end{aligned} \tag{4.29a}$$

$$E_p = \frac{1}{2}\kappa(\psi_g - \psi^0_g)^2 + \frac{1}{2}\kappa(\vartheta_g - \vartheta^0_g)^2. \tag{4.29b}$$

The Lagrange function has the following form:

$$L = E_k - E_P. \tag{4.30}$$

Taking into account the fact that a generalized coordinate Φ_g is cyclic, we obtain equations of motion of the gyroscope in the following form:

1. Equations of motion of the gyroscope axis

$$\begin{aligned}
&I^0_{X''_2}\frac{\mathrm{d}}{\mathrm{d}t}(\omega^0_{gX'_2}\cos^2\vartheta^0_g) + m_2\cdot l_g^2(1+\cos\vartheta^0_g)^2\frac{\mathrm{d}\omega^0_{gX'_2}}{\mathrm{d}t} + I^0_{X''_1}\omega^0_{gX''_1}\omega^0_{gX'_3}\\
&\quad + \frac{1}{2}I^0_{X''_2}\omega^0_{gX'_3}\Big[\sin 2\vartheta^0_g + (\omega^0_{gX''_1} - \omega^0_{gX'_1})\cos^2\vartheta^0_g\Big] - \kappa(\psi_g - \psi^0_g)\\
&\quad + m_2 l_g\Big\{(1+\cos\vartheta^0_g)\cdot(\dot{u}_s\cos\psi^0_g - (\dot{w}_s - \dot{q}^* l_s)\sin\psi^0_g)\\
&\quad - \dot{\psi}^0_g\Big[u_s\sin\psi^0_g + (w_s - q^* l_s)\cos\psi^0_g\Big] - V^0_{gX''_1}\dot{\vartheta}^0_g\sin\vartheta^0_g\Big\}\\
&\quad + m_2 l_g^2\Big[(\omega^0_{gX'_2} + \omega^0_{gX''_2})\omega^0_{gX'_1}\sin\vartheta^0_g - (1+\cos\vartheta^0_g)\omega^0_{gX''_1}\omega^0_{gX'_3}\\
&\quad + \dot{\vartheta}^0_g\omega^0_{gX''_3} + \dot{\omega}^0_{gX'_3}\sin\vartheta^0_g\Big] + m_2 l_s l_g\Big\{q_s\Big[(\omega^0_{gX'_1} - \omega^0_{gX''_1})\sin\psi^0_g\sin\vartheta^0_g\\
&\quad + (\omega^0_{gX'_2} + \omega^0_{gX''_3})\cos\psi^0_g - \omega^0_{gX'_3}\cos\Psi^0_g\sin\vartheta^0_g\cos\vartheta^0_g\Big]\\
&\quad + (1+\cos\vartheta^0_g)\cdot r^*\omega^0_{gX'_3}\Big\} = M_c - M_{rc},
\end{aligned} \tag{4.31}$$

$$\begin{aligned}
&I^0_{X''_1}\frac{\mathrm{d}\omega^0_{gX''_1}}{\mathrm{d}t} + m_2 l_g^2\ddot{\vartheta}^0_g - I^0_{X''_2}\omega^0_{gX''_2}\omega^0_{gX''_3} - \kappa(\vartheta_g - \vartheta^0_g)\\
&\quad - m_2 l_g\Big\{\Big[\dot{\psi}^0_g(u_s\cos\psi^0_g - (w_s - q^* l_s)\sin\psi^0_g) + \dot{u}_s\sin\psi^0_g\\
&\quad + (w_s - \dot{q}^* l_s)\cos\psi^0_g\Big]\sin\vartheta^0_g + \dot{\vartheta}^0_g V^0_{gX''_3} + \dot{v}_s\cos\vartheta^0_g\\
&\quad - \Big[q^*(\omega^0_{gX''_3}\sin\psi^0_g + \omega^0_{gX''_1}\cos\psi^0_g\cos\vartheta^0_g) + r^*\omega^0_{gX''_1}\sin\vartheta^0_g - \dot{r}^*\cos\vartheta^0_g\Big]\cdot l_s\\
&\quad - \Big[(\omega^0_{gX'_2} + \omega^0_{gX''_2})\omega^0_{gX''_3} - \omega^0_{gX'_1}\omega^0_{gX''_1}\sin\vartheta^0_g + (1+\cos\vartheta^0_g)\dot{\omega}^0_{gX'_1}\Big]\cdot l_g\Big\}\\
&\quad = M_b - M_{rb}.
\end{aligned} \tag{4.32}$$

2. Equations of motion of gyroscope rotor

$$
\begin{aligned}
&\Bigg[I_{X_2'} + I^*_{X_2''} + I^*_{X_2'''} + (I^*_{X_3''} - I^*_{X_2''} - I^*_{X_2'''})\sin^2\vartheta_g \\
&\quad + m_3 l_g^2(1+\cos\vartheta_g)^2\Bigg]\frac{\mathrm{d}\omega_{gX_2'}}{\mathrm{d}t} + \frac{I^*_{X_3''} - I^*_{X_2''} - I^*_{X_2'''}}{2}(\omega_{gX_2'}\dot{\vartheta}_g \\
&\quad - \dot{\omega}_{gX_3'})\sin 2\vartheta_g - (I_{X_3'} - I_{X_1'})\cdot\omega_{gX_1'}\omega_{gX_3'} \\
&\quad + I^*_{X_1'''}\omega_{gX_1''}\omega_{gX_3'} + \Bigg[I^*_{X_2''} + I^*_{X_2'''} + (I^*_{X_3''} - I^*_{X_2''} \\
&\quad - I^*_{X_2'''})\sin^2\vartheta_g\Bigg]\cdot\dot{\vartheta}_g\omega_{gX_3'} - \Bigg[(I^*_{X_2''} + I^*_{X_2'''})\cdot\omega_{gX_1''}\omega_{gX_2''} \\
&\quad + I^*_{X_3'''}\dot{\omega}_{gX_3'''}\Bigg]\sin\vartheta_g - \Bigg[I^*_{X_3''}\omega_{gX_3''} + I^*_{X_3'''}(\omega_{gX_3''} + \dot{\Phi}_g)\Bigg] \\
&\qquad \times\omega_{gX_1''}\cos\vartheta_g + m_3 l_g\Bigg\{(1+\cos\vartheta_g)\cdot\Bigg[\dot{u}_s\cos\psi_g \\
&\quad - (\dot{w}_s - \dot{q}^* l_s)\sin\psi_g\Bigg] - \dot{\psi}_g\Bigg[u_s\sin\psi_g + (w_s - q^* l_s)\cos\psi_g\Bigg] \\
&\quad - V_{gX_1''}\dot{\vartheta}_g\sin\vartheta_g\Bigg\} + m_3 l_g^2\Bigg[(\omega_{gX_2'} + \omega_{gX_2''})\omega_{gX_1'}\sin\vartheta_g \\
&\quad - (1+\cos\vartheta_g)\omega_{gX_1''}\omega_{gX_3'} + \dot{\vartheta}_g\omega_{gX_3''} + \dot{\omega}_{gX_3'}\sin\vartheta_g\Bigg] \\
&\quad + m_3 l_s l_g\Bigg\{q^*\Bigg[(\omega_{gX_1'} - \omega_{gX_1''})\sin\psi_g\sin\vartheta_g \\
&\quad + (\omega_{gX_2'} + \omega_{gX_3''})\cos\psi_g - \omega_{gX_3'}\cos\psi_g\sin\vartheta_g\cos\vartheta_g\Bigg] \\
&\quad + (1+\cos\vartheta_g)\cdot r^*\omega_{gX_3'}\Bigg\} + \kappa(\psi_g - \psi_g^0) = M_{zc},
\end{aligned}
\tag{4.33}
$$

$$
\begin{aligned}
&(I^*_{X_1''} + I^*_{X_1'''})\frac{\mathrm{d}\omega_{gX_1''}}{\mathrm{d}t} + m_3\cdot l_g^2\ddot{\vartheta}_g + (I^*_{X_3''} - I^*_{X_2''} - I^*_{X_2'''})\cdot\omega_{gX_2''}\omega_{gX_3''} \\
&\quad + I^*_{X_3'''}(\omega_{gX_3''} + \dot{\Phi}_g)\cdot\omega_{gX_2''} + \kappa(\vartheta_g - \vartheta_g^0) \\
&\quad - m_3 l_g\Bigg\{\Bigg[\dot{\psi}_g(u_s\cos\psi_g - (w_s - q^* l_s)\sin\psi_g) + \dot{u}_s\sin\psi_g \\
&\quad + (w_s - q^* l_s)\cos\psi_g\Bigg]\sin\vartheta_g + \dot{\vartheta}_g V_{gX_3''} + \dot{v}_s\cos\vartheta_g
\end{aligned}
$$

$$-\Big[q^*(\omega_{gX_3''}\sin\psi_g+\omega_{gX_1''}\cos\psi_g\cos\vartheta_g)+r^*\omega_{gX_1''}\sin\vartheta_g$$
$$-\dot{r}^*\cos\vartheta_g\Big]\cdot l_s-\Big[(\omega_{gX_2'}+\omega_{gX_2''})\cdot\omega_{gX_3''}-\omega_{gX_1'}\omega_{gX_1''}\sin\vartheta_g$$
$$+(1+\cos\vartheta_g)\cdot\dot{\omega}_{gX_1'}\Big]\cdot l_g\Big\}=M_{zb}, \tag{4.34}$$

$$I^*_{X_3'''}\frac{\mathrm{d}}{\mathrm{d}t}(\omega_{gX_3''}+\dot{\Phi}_g)=M_k-M_{rk}, \tag{4.35}$$

where

$$\dot{\omega}^0_{gX_1'}=\frac{\mathrm{d}\omega^0_{gX_1'}}{\mathrm{d}t}=\dot{p}^*\cos\psi^0_g-p^*\dot{\psi}^0_g\sin\psi^0_g-\dot{r}^*\sin\psi^0_g-r^*\cos\psi^0_g,$$

$$\dot{\omega}^0_{gX_3'}=\frac{\mathrm{d}\omega^0_{gX_3'}}{\mathrm{d}t}=\dot{p}^*\sin\psi^0_g+p^*\dot{\psi}^0_g\cos\psi^0_g+\dot{r}^*\cos\psi^0_g-r^*\sin\psi^0_g.$$

The preceding mathematical model of gyroscope motion, along with the equations of motion of the base (board of FO) on which the gyroscope is set, makes it possible to perform large-scale simulation investigations of gyroscope dynamics. Moreover, the presented form of equations has the most general and universal character. From these equations it is possible to derive all other equations describing the known types of gyroscopes. It should be emphasized that in the model governed by (4.31)–(4.35), deformability of the rotor is taken into account (elasticity coefficient κ) as is the position of the center of mass of the gyroscope at some distance l_s from the center of mass of the OL (which can matter in the case of a non-astatic gyroscope). Since no known analytical methods of solving the derived equations exist, investigation of the model will be performed by means of numerical methods. The universality of (4.31)–(4.35) relies on the fact that by ignoring specific terms of particular equations, it is possible to obtain the desired gyroscope models. In the next subsection, we will present an example of transformation of the aforementioned equations into forms describing a model of a classic, controlled gyroscope on a fixed base.

4.1.1 Astatic Gyroscope on a Fixed Platform with Axis Stiff-Connected to Rotor

Suppose that a gyroscope is located on a fixed base, which implies that $u_s=0$, $v_s=0$, $w_s=0$, $p_s=0$, $q_s=0$, $r_s=0$. We do not take into account the rotational motion of the Earth, and we assume that the gyroscope is astatic, i.e., the distance

of the center of mass of the system rotor's internal frame $l_g = 0$. The equations of motion of the gyroscope take the form

$$I^0_{X_2''}\frac{\mathrm{d}^2\psi_g^0}{\mathrm{d}t^2}\cos^2\vartheta_g^0 - I^0_{X_2''}\dot{\psi}_g^0\dot{\vartheta}_g^0\sin 2\vartheta_g^0 - \kappa(\psi_g - \psi_g^0) = M_c - M_{rc}, \quad (4.36a)$$

$$I^0_{X_1''}\frac{\mathrm{d}^2\vartheta_g^0}{\mathrm{d}t^2} + \tfrac{1}{2}I^0_{X_2''}(\dot{\psi}_g^0)^2\sin 2\vartheta_g^0 - \kappa(\vartheta_g - \vartheta_g^0) = M_b - M_{rb}, \quad (4.36b)$$

$$\begin{aligned}&\left[I_{X_2'} + I^*_{X_2''} + I^*_{X_2'''} + (I^*_{X_3''} - I^*_{X_2''} - I^*_{X_2'''})\sin^2\vartheta_g\right]\frac{\mathrm{d}^2\psi_g}{\mathrm{d}t^2}\\ &\quad + (I^*_{X_3''} - I^*_{X_2''} - I^*_{X_2'''})\cdot\dot{\psi}_g\dot{\vartheta}_g\sin 2\vartheta_g\\ &\quad - I^*_{X_3'''}\frac{\mathrm{d}}{\mathrm{d}t}(\dot{\Phi}_g - \dot{\psi}_g\sin\vartheta_g)\sin\vartheta_g\\ &\quad - I^*_{X_3'''}(\dot{\Phi}_g - \dot{\psi}_g\sin\vartheta_g)\dot{\vartheta}_g\cos\vartheta_g + \kappa(\psi_g - \psi_g^0) = M_{zc}, \end{aligned} \quad (4.37)$$

$$\begin{aligned}&(I^*_{X_1''} + I^*_{X_1'''})\frac{\mathrm{d}^2\vartheta_g}{\mathrm{d}t^2} - \frac{1}{2}(I^*_{X_3''} - I^*_{X_2''} - I^*_{X_2'''})\dot{\psi}_g^2\sin 2\vartheta_g + \kappa(\vartheta_g - \vartheta_g^0)\\ &\quad + I^*_{X_3'''}(\dot{\Phi}_g - \dot{\psi}_g\sin\vartheta_g)\dot{\psi}_g\cos\vartheta_g = M_{zb}, \end{aligned} \quad (4.38)$$

$$I_{X_3'''}\frac{\mathrm{d}}{\mathrm{d}t}(\dot{\Phi}_g - \dot{\psi}_g\sin\vartheta_g) = M_k - M_{rk}. \quad (4.39)$$

Equations (4.36a) and (4.36b) yield

$$(\psi_g - \psi_g^0) = \frac{I^0_{X_2''}\frac{\mathrm{d}^2\psi_g^0}{\mathrm{d}t^2}\cos^2\vartheta_g - I^0_{X_2''}\dot{\psi}_g^0\dot{\vartheta}_g^0\sin 2\vartheta_g^0 - M_c + M_{rc}}{\kappa}, \quad (4.40a)$$

$$(\vartheta_g - \vartheta_g^0) = \frac{I^0_{X_1''}\frac{\mathrm{d}^2\vartheta_g^0}{\mathrm{d}t^2} + \frac{1}{2}I^0_{X_2''}(\dot{\psi}_g^0)^2\sin 2\vartheta_g^0 - M_b + M_{rb}}{\kappa}. \quad (4.40b)$$

Substituting (4.40a) into (4.37) and (4.40b) into (4.38), one obtains

$$\begin{aligned}&\left[I_{X_2'} + I^*_{X_2''} + I^*_{X_2'''} + (I^*_{X_3''} - I^*_{X_2''} - I^*_{X_2'''})\sin^2\vartheta_g\right]\frac{\mathrm{d}^2\psi_g}{\mathrm{d}t^2}\\ &\quad + (I^*_{X_3''} - I^*_{X_2''} - I^*_{X_2'''})\dot{\psi}_g\dot{\vartheta}_g\sin 2\vartheta_g - I^*_{X_3'''}\frac{\mathrm{d}}{\mathrm{d}t}(\dot{\Phi}_g - \dot{\psi}_g\sin\vartheta_g)\sin\vartheta_g\end{aligned}$$

$$- I^*_{X'''_3}(\dot{\Phi}_g - \dot{\psi}_g \sin\vartheta_g)\dot{\vartheta}_g \cos\vartheta_g + I^0_{X''_2}\frac{\mathrm{d}^2\psi^0_g}{\mathrm{d}t^2}\cos^2\vartheta_g$$
$$- I^0_{X''_2}\dot{\psi}^0_g\dot{\vartheta}^0_g \sin 2\vartheta^0_g = M_{zc} + M_c - M_{rc}, \tag{4.41}$$

$$(I^*_{X''_1} + I^*_{X'''_1})\frac{\mathrm{d}^2\vartheta_g}{\mathrm{d}t^2} - \frac{1}{2}(I^*_{X''_3} - I^*_{X''_2} - I^*_{X'''_2})\dot{\psi}^2_g \sin 2\vartheta_g$$
$$+ I^0_{X''_1}\frac{\mathrm{d}^2\vartheta^0_g}{\mathrm{d}t^2} + I^*_{X'''_3}(\dot{\Phi}_g - \dot{\psi}_g \sin\vartheta_g)\dot{\psi}_g \cos\vartheta_g$$
$$+ \frac{1}{2}I^0_{X''_2}(\dot{\psi}^0_g)^2 \sin 2\vartheta^0_g = M_{zb} + M_b - M_{rb}. \tag{4.42}$$

Consider the case where the stiffness coefficient $\kappa \to \infty$. It follows from (4.40a) and (4.40b) that

$$\psi^0_g \approx \psi_g \quad \text{and} \quad \vartheta^0_g \approx \vartheta_g. \tag{4.43}$$

Thus, we obtained constraint equations for (4.37) and (4.38). This means that the axis will be stiff-connected to the gyroscope rotor. Taking into account constraints (4.43), (4.41) and (4.42) take the form

$$\left[I_{X'_2} + I_{X''_3} + (I_{X''_2} + I^0_{X''_2} + I_{X'''_2} - I_{X''_3})\cos^2\vartheta_g\right]\frac{\mathrm{d}^2\psi_g}{\mathrm{d}t^2}$$
$$- (I_{X''_2} + I^0_{X''_2} + I_{X'''_2})\dot{\psi}_g\dot{\vartheta}_g \sin 2\vartheta_g$$
$$- I_{X'''_3}\frac{\mathrm{d}}{\mathrm{d}t}(\dot{\Phi}_g - \dot{\psi}_g \sin\vartheta_g)\sin\vartheta_g + I_{X'''_3}(\dot{\Phi}_g - \dot{\psi}_g \sin\vartheta_g)\dot{\vartheta}_g \cos\vartheta_g$$
$$= M_{zc} + M_c - M_{rc}, \tag{4.44}$$

$$(I_{X''_1} + I^0_{X''_1} + I_{X'''_1})\frac{\mathrm{d}^2\vartheta_g}{\mathrm{d}t^2} + \frac{1}{2}(I_{X''_2} + I^0_{X''_2} + I_{X'''_2} - I_{X''_3})\dot{\psi}^2_g \sin 2\vartheta_g$$
$$+ I_{X'''_3}(\dot{\Phi}_g - \dot{\psi}_g \sin\vartheta_g)\dot{\psi}_g \cos\vartheta_g = M_{zb} + M_b - M_{rb}. \tag{4.45}$$

If we ignore the inertia of the frames $I_{X''_1} = 0$, $I^0_{X''_1} = 0$, $I_{X''_2} = 0$, $I^0_{X''_2} = 0$, $I_{X'_2} = 0$, $I_{X''_3} = 0$ and the values of the disturbing torques $M_{zb} = 0$ and $M_{zc} = 0$, and if we introduce additional designations (bearing in mind that the rotor is axially symmetric), then $I_{X'''_1} = I_{X'''_2} = I_{gk}$, $I_{X'''_3} = I_{go}$, then formulas (4.41) and (4.42) are cast to the following form

$$I_{gk}\frac{\mathrm{d}^2\psi_g}{\mathrm{d}t^2}\cos^2\vartheta_g - I_{gk}\dot{\psi}_g\dot{\vartheta}_g \sin 2\vartheta_g - I_{go}(\dot{\Phi}_g - \dot{\psi}_g \sin\vartheta_g)\dot{\vartheta}_g \cos\vartheta_g$$
$$= M_c + M_k - M_{rc}, \tag{4.46a}$$

$$I_{gk}\frac{\mathrm{d}^2\vartheta_g}{\mathrm{d}t^2}+\frac{1}{2}I_{gk}\dot{\psi}_g^2\sin 2\vartheta_g+I_{go}(\dot{\Phi}_g-\dot{\psi}_g\sin\vartheta_g)\dot{\psi}_g\cos\vartheta_g=M_b-M_{rb}. \quad (4.46b)$$

Suppose that the torque driving the rotor is equal to the moment of friction forces in the rotor bearings and aerodynamic resistance

$$M_k=M_{rk}, \quad (4.47a)$$

and hence

$$\frac{\mathrm{d}\Phi_g}{\mathrm{d}t}-\dot{\psi}_g\sin\vartheta_g=\mathrm{const}=n_g. \quad (4.47b)$$

Finally, taking into account (4.47a), (4.47b) will take the form

$$I_{gk}\frac{\mathrm{d}^2\psi_g}{\mathrm{d}t^2}\cos^2\vartheta_g-I_{gk}\dot{\psi}_g\dot{\vartheta}_g\sin 2\vartheta_g-I_{go}n_g\dot{\vartheta}_g\cos\vartheta_g=M_c-M_{rc}, \quad (4.48a)$$

$$I_{gk}\frac{\mathrm{d}^2\vartheta_g}{\mathrm{d}t^2}+\frac{1}{2}I_{gk}\dot{\psi}_g^2\sin 2\vartheta_g+I_{go}n_g\dot{\psi}_g\cos\vartheta_g=M_b-M_{rb}. \quad (4.48b)$$

We have obtained equations of motion of a classic gyroscope on a fixed base with the axis stiff-connected to the rotor.

Numerical investigations to be carried out later on in this work for systems describing gyroscope motion [such as (4.75a)], it is convenient to perform, not for a real time t, but for a "dimensionless" τ, which is determined as follows [5, 6, 8]:

$$\tau=\Omega\cdot t, \quad (4.49)$$

where

$$\Omega=\frac{I_{go}n_g}{I_{gk}}.$$

Rescaling time one obtains

$$\frac{\mathrm{d}}{\mathrm{d}t}=\frac{\mathrm{d}}{\mathrm{d}\tau}\frac{\mathrm{d}\tau}{\mathrm{d}t}=\Omega\frac{\mathrm{d}}{\mathrm{d}\tau} \quad (4.50)$$

and

$$\dot{\vartheta}_g=\Omega\frac{\mathrm{d}\vartheta_g}{\mathrm{d}\tau}=\Omega\vartheta_g', \qquad \ddot{\vartheta}_g=\Omega^2\frac{\mathrm{d}^2\vartheta_g}{\mathrm{d}\tau^2}=\Omega^2\vartheta_g'', \quad (4.51a)$$

and similarly

$$\dot{\psi}_g=\Omega\cdot\psi_g', \qquad \ddot{\psi}_g=\Omega^2\psi_g''. \quad (4.51b)$$

The change in time scale in the preceding examples makes the numerical analysis of the equation of motion easier because the change makes values of the equation elements equal and allows us to introduce a greater integration step. This makes numerical errors smaller.

Applying the dimensionless time τ in (4.48a)–(4.48b) and taking into account (4.50), (4.51a), and (4.51b) one finds

$$\frac{\mathrm{d}^2\psi_g}{\mathrm{d}\tau^2}\cos^2\vartheta_g - \psi_g'\vartheta_g'\sin 2\vartheta_g + b_b\psi_g' - \vartheta_g'\cos\vartheta_g = c_b M_c, \tag{4.52a}$$

$$\frac{\mathrm{d}^2\vartheta_g}{\mathrm{d}\tau^2} + \frac{1}{2}(\psi_g')^2\sin 2\vartheta_g + b_c\vartheta_g' + \psi_g'\cos\vartheta_g = c_c M_b, \tag{4.52b}$$

where

$$b_b = \frac{\eta_b}{I_{gk}\Omega}, \quad b_c = \frac{\eta_c}{I_{gk}\Omega}, \quad c_b = \frac{1}{I_{gk}\Omega^2}, \quad c_c = \frac{1}{I_{gk}\Omega^2}.$$

4.1.2 *Simplified Equations (Technical) of Motion of a Gyroscope*

Analysis of (4.48) and (4.52) is very troublesome because of the difficulties in obtaining analytical solutions. System (4.48) is strongly non-linear, which is why its solution can be obtained only by means of numerical methods. However, the system can be simplified considerably if we eliminate terms that have a slight effect on the motion character of the gyroscope.

Note that the value of the angular velocity of eigenrotations $\dot{\Phi}_g$ of the gyroscope is incomparably greater than the value of the velocities $\dot{\vartheta}_g$ and $\dot{\psi}_g$ of rotations of the internal and external frames. Hence, in (4.48) we can leave out those terms that include products $\dot{\vartheta}_g$ and $\dot{\psi}_g$ or their squares as higher-order quantities of smallness. Moreover, if we consider a fixed range of rotor operation corresponding to balancing the driving torque M_k with the resistance torques M_{rk}, i.e., an almost constant angular velocity of the eigenrotations of the gyroscope, $\dot{\Phi}_g \cong \text{const} = n_g$, then (4.48) will take the following forms:

$$I_{gk}\frac{\mathrm{d}^2\vartheta_g}{\mathrm{d}t^2} + I_{go}n_g\dot{\psi}_g\cos\vartheta_g = M_b - M_{rb}, \tag{4.53a}$$

$$I_{gk}\frac{\mathrm{d}^2\psi_g}{\mathrm{d}t^2} - I_{go}n_g\dot{\vartheta}_g\cos\vartheta_g = M_c - M_{rc}. \tag{4.53b}$$

The preceding forms of equations, governing the motion of a gyroscope about a fixed point of its suspension, are called *technical equations* or the *technical theory* of the *gyroscope* [7, 9, 10].

Taking into account the fact that (as was earlier assumed) angular velocities $\dot{\vartheta}_g$ and $\dot{\psi}_g$ have small values and assuming that the initial conditions equal zero, one can assume, with sufficient accuracy from a practical viewpoint, that $\cos\vartheta_g \cong 1$. If we assume that the moments of friction forces in the frame bearings are small, i.e., $M_{rb} = 0$, $M_{rc} = 0$, then (4.53) will take simpler, final forms:

$$I_{gk}\frac{\mathrm{d}^2\vartheta_g}{\mathrm{d}t^2} + I_{go}n_g\dot{\psi}_g = M_b, \tag{4.54a}$$

$$I_{gk}\frac{\mathrm{d}^2\psi_g}{\mathrm{d}t^2} - I_{go}n_g\dot{\vartheta}_g = M_c. \tag{4.54b}$$

4.1.3 Remarks on the Model of Gyroscopic Motion

The most general mathematical model of a controlled gyroscope has been derived. It follows from the literature overview that the complete numerical investigations of the dynamics of the controlled gyroscope have not been performed satisfactorily, especially when the full equations describing the motion of a gyroscope base (e.g., board of a FO) are taken into account. This option is ensured by the model given in this chapter and governed by (4.31)–(4.35). In particular, it makes it possible to examine the influence of the following factors on the accuracy of maintaining the preset motion (position) in space by the gyroscope axis:

1. Inertia of suspension frames.
2. Distance l_g between the center of mass of the gyroscope and the center of its rotation (unbalanced gyroscope).
3. Distances l_s between the center of mass of the gyroscope and the center of mass of the FO.
4. Stiffness κ of the element connecting the rotor to the gyroscope axis.
5. Kinematic excitations in the form of linear u_s, v_s, w_s and angular p_s, q_s, r_s velocities (and their first derivatives with respect to time) affecting the gyroscope suspension.
6. Rotational motion of the Earth.

The generality of the model enables us to analyze various types of gyroscopes by means of elimination of appropriate terms in (4.31)–(4.35). Thus, one could pass from the description of a non-astatic gyroscope on an elastic suspension to a classic description of an astatic gyroscope.

The computing power of today's computers allows one, in a relatively simple way, to verify the results obtained thus far of the theoretical investigations of gyroscopes—reduced to simplified models in most cases—with the results obtained from numerical simulations of a completely non-linear model.

4.2 Gyroscope Control

The motion of a gyroscope axis can be realized under the influence of the controlling torques M_b and M_c and angular motion of its base, determined by angular velocities $p^*(t)$, $q^*(t)$, and $r^*(t)$, or the linear movements of its base (in the case of a

non-astatic gyroscope), determined by linear velocities $u_s(t)$, $v_s(t)$, and $w_s(t)$. While the torques cause the excitation of motion of a gyroscope axis by external forces, the angular and linear velocities of the base reflect the parametrical excitation of the motion.

In this subsection, we will consider programmable control of motion of a gyroscope axis in an open system and corrective and stabiling control of motion of a gyroscope axis in a closed system. We will examine the effect of gyroscope errors on the realization of preset motion. Moreover, we will give optimal control algorithms of position of a gyroscope axis relative to a preset trajectory.

4.2.1 Motion Control of Gyroscope Axis in an Open System: The Inverse Problem in Gyroscope Dynamics

The inverse problem of a gyroscope relies on determining the torques $M_b(t)$ and $M_c(t)$ that, acting on the gyroscope frames, will set the gyroscope axis in motion, specified by the angles $\vartheta_{gz}(t)$ and $\psi_{gz}(t)$. Thus, the problem is reduced to determining programs according to which the torques $M_b(t)$ and $M_c(t)$ are to change in time, i.e., the programmable control of the gyroscope axis motion in an open system [11–13].

In order to determine the torques $M_b(t)$ and $M_c(t)$ we make use of the general definition, which says that inverse problems of dynamics are called problems that rely on *determining the external forces, the parameters of this system, and the constraints imposed on the system at which motion with preset properties is the only motion among all possible motions*. In practice, these problems refer to the particular cases relying on formulating the algorithms that determine the controlling forces and realize the desired motion of a dynamical system—regardless of the problem conditions—though they are not always achieved.

Thus, the inverse problem relies on task of runs as functions of time $\vartheta_g = \vartheta_g(t)$ and $\psi_g = \psi_g(t)$, substituting them into the left-hand sides of the equations of motion of a gyroscope axis and evaluating $M_b(t)$ and $M_c(t)$ (i.e., the right-hand sides of these equations). The determined torques M_b and M_c, plugged into the right-hand sides of the equations of motion, give a unique (appropriate) result only for the angular velocities $\dot{\vartheta}_g(t)$ and $\dot{\psi}_g(t)$, while only for the angles will the result not be unique in general since it depends on integration constants of the angles' derivatives. This can be compensated by appropriate selection of the integration constants in the solution to the equations.

This implies that the determined $M_b(t)$ and $M_c(t)$, on the basis of the inverse problem solution, can be used to programmatically control only of the derivatives angles and not the angles of the gyroscope position. A scheme for an algorithm to control a gyroscope in an open system is depicted in Fig. 4.2.

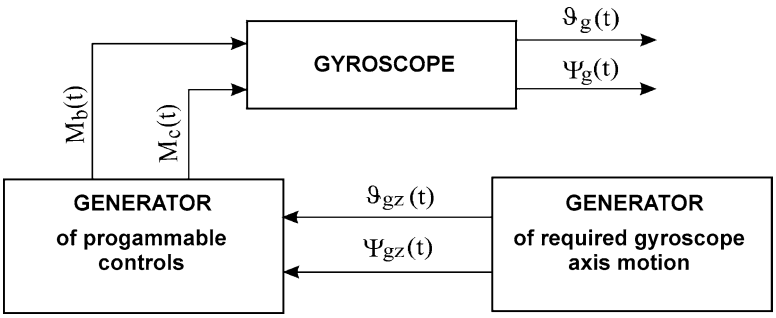

Fig. 4.2 Scheme of algorithm for controlling a gyroscope in an open system

Consider the following problem: let a gyroscope axis describe the a surface of a cone (Fig. 4.3a). Then the following equations must be satisfied:

$$\begin{aligned} \vartheta_{gz}(t) &= \Theta_k \sin \nu_k t, & \psi_{gz}(t) &= \Theta_k \cos \nu_k t, \\ \frac{\vartheta_{gz}}{\mathrm{d}t} &= \Theta_k \nu_k \cos \nu_k t, & \frac{\psi_{gz}}{\mathrm{d}t} &= -\Theta_k \nu_k \sin \nu_k t, \\ \frac{\mathrm{d}^2\vartheta_{gz}}{\mathrm{d}t^2} &= -\Theta_k \nu_k^2 \sin \nu_k t, & \frac{\mathrm{d}^2\psi_{gz}}{\mathrm{d}t^2} &= -\Theta_k \nu_k^2 \cos \nu_k t. \end{aligned} \tag{4.55}$$

Let us make use of the linearized equations of a gyroscope (4.53b)–(4.53b) in which we suppose that $\Theta_g \ll 1$ and the friction in the suspension bearings is of a viscous type. Then they will have the following form [14–16]:

$$\begin{aligned} \frac{\mathrm{d}^2\vartheta_g}{\mathrm{d}t^2} + \eta_b \Omega \frac{\mathrm{d}\vartheta_g}{\mathrm{d}t} - \Omega \frac{\mathrm{d}\psi_g}{\mathrm{d}t} &= \frac{M_b}{I_{gk}}, \\ \frac{\mathrm{d}^2\psi_g}{\mathrm{d}t^2} + \eta_c \Omega \frac{\mathrm{d}\psi_g}{\mathrm{d}t} + \Omega \frac{\mathrm{d}\vartheta_g}{\mathrm{d}t} &= \frac{M_c}{I_{gk}}. \end{aligned} \tag{4.56}$$

Substituting (4.55) into the left-hand side of (4.56) we obtain

$$\begin{aligned} \frac{\mathrm{d}^2\vartheta_{gz}}{\mathrm{d}t^2} + \eta_b \Omega \frac{\mathrm{d}\vartheta_{gz}}{\mathrm{d}t} - \Omega \frac{\mathrm{d}\psi_{gz}}{\mathrm{d}t} &= \Theta_k \nu_k (\Omega - \nu_k) \sin \nu_k t + \eta_b \Theta_k \nu_k \Omega \cos \nu_k t, \\ \frac{\mathrm{d}^2\psi_{gz}}{\mathrm{d}t^2} + \eta_c \Omega \frac{\mathrm{d}\psi_{gz}}{\mathrm{d}t} + \Omega \frac{\mathrm{d}\vartheta_{gz}}{\mathrm{d}t} &= \Theta_k \nu_k (\Omega - \nu_k) \cos \nu_k t - \eta_c \Theta_k \nu_k \Omega \sin \nu_k t, \end{aligned} \tag{4.57}$$

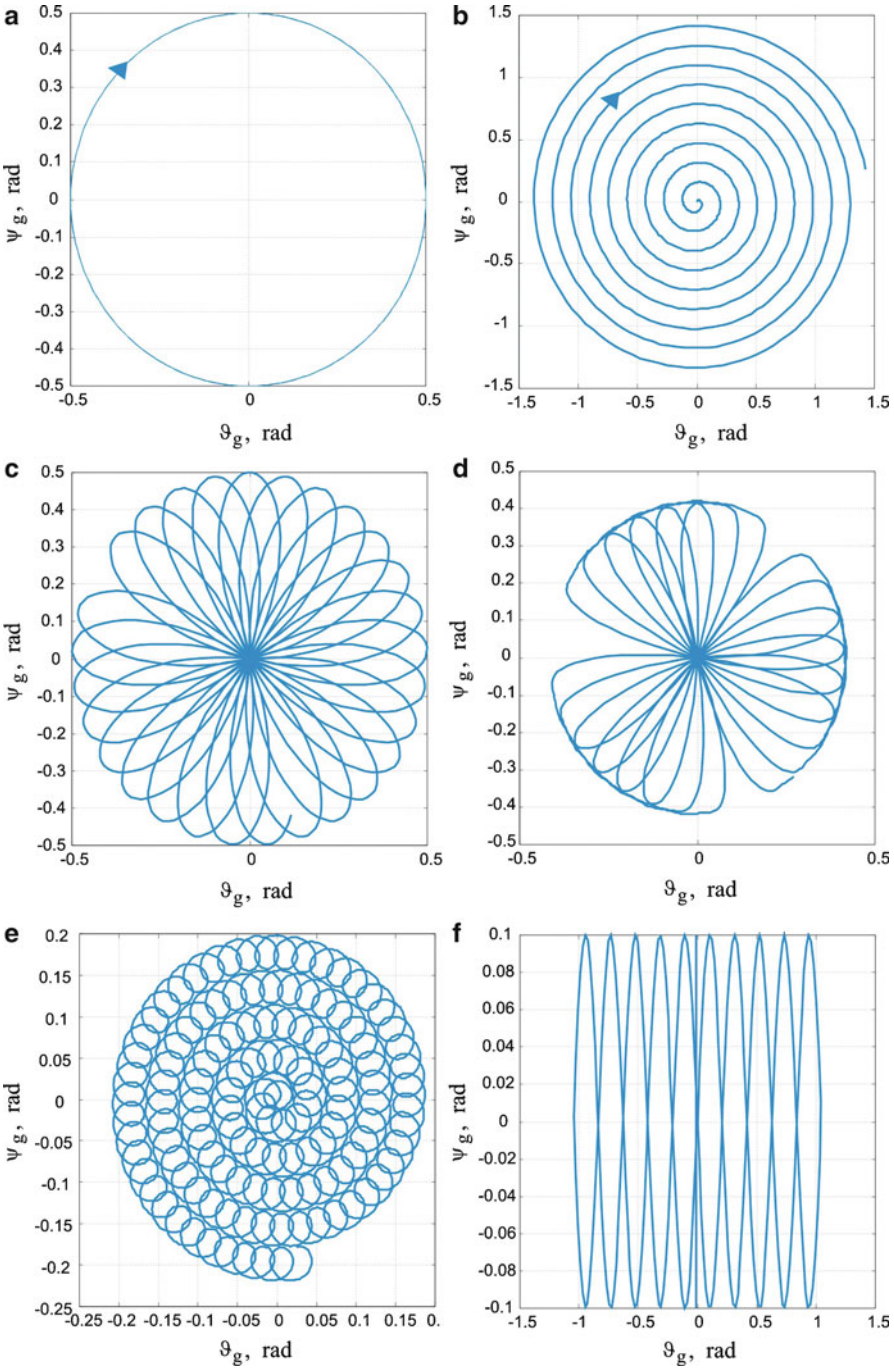

Fig. 4.3 Examples of curves drawn by the gyroscope axis: (**a**) on a cone surface, (**b**) along Archimedes spiral, (**c**) *n*-flute rosette, (**d**) modified n-flute rosette, (**e**) described by (4.67), (**f**) described by (4.68)

and hence

$$M_b = I_{gk}[\Theta_k \nu_k(\Omega - \nu_k)\sin \nu_k t + \eta_b \Theta_k \nu_k \Omega \cos \nu_k t],$$
$$M_c = I_{gk}[\Theta_k \nu_k(\Omega - \nu_k)\cos \nu_k t - \eta_b \Theta_k \nu_k \Omega \sin \nu_k t]. \tag{4.58}$$

Thus, we have the torques $M_b(t)$ and $M_c(t)$ determined as functions of time. Now let us check what trajectory will be generated by these torques. Let us substitute them into the right-hand sides of (4.56):

$$\frac{\mathrm{d}^2\vartheta_g}{\mathrm{d}t^2} + \eta_b\Omega\frac{\mathrm{d}\vartheta_g}{\mathrm{d}t} - \Omega\frac{\mathrm{d}\psi_g}{\mathrm{d}t} = \Theta_k \nu_k(\Omega - \nu_k)\sin \nu_k t + \eta_b \Theta_k \nu_k \Omega \cos \nu_k t,$$
$$\frac{\mathrm{d}^2\psi_g}{\mathrm{d}t^2} + \eta_c\Omega\frac{\mathrm{d}\psi_g}{\mathrm{d}t} + \Omega\frac{\mathrm{d}\vartheta_g}{\mathrm{d}t} = \Theta_k \nu_k(\Omega - \nu_k)\cos \nu_k t - \eta_c \Theta_k \nu_k \Omega \sin \nu_k t. \tag{4.59}$$

The inverse problem is unique for the derivatives of angles ϑ_g and ψ_g with respect to time, but for stationary motion [17, 18], i.e., as $t \to \infty$ (a transient process is depicted in Figs. 4.6b and 4.7b). However, that question arises as to whether the solutions to the preceding equations will also describe the preset motion of the gyroscope axis. If we impose the initial angular position of the axis as required, $\vartheta_{gz}(0) = 0$ and $\psi_{gz}(0) = \Theta_k$, then we will obtain the required angular displacements of the gyroscope axis. If, however, the initial position of the axis is not the one we need, e.g., $\vartheta_{gz}(0) = 0.1$ rad and $\psi_{gz}(0) = 0.1$ rad, then despite the fact that the angular velocities are the ones we need, the gyroscope axis does not describe the required surface (Figs. 4.5 and 4.7).

In the case of angular deviations taking large values of the gyroscope axis, the control moments $M_b(\tau)$ and $M_c(\tau)$, as functions of non-dimensional time τ, are determined from the non-linear (4.52a)–(4.52b):

$$M_b(\tau) = \frac{\mathrm{d}^2\vartheta_{gz}}{\mathrm{d}\tau^2} + b_b\frac{\mathrm{d}\vartheta_{gz}}{\mathrm{d}\tau} + \frac{1}{2}\left(\frac{\mathrm{d}\psi_{gz}}{\mathrm{d}\tau}\right)^2 \sin 2\vartheta_{gz} + \frac{\mathrm{d}\psi_{gz}}{\mathrm{d}\tau}\cos\vartheta_{gz}, \tag{4.60}$$

$$M_c(\tau) = \frac{\mathrm{d}^2\psi_{gz}}{\mathrm{d}\tau^2}\cos^2\vartheta_{gz} + b_c\frac{\mathrm{d}\psi_{gz}}{\mathrm{d}\tau} - \frac{\mathrm{d}\psi_{gz}}{\mathrm{d}\tau}\frac{\mathrm{d}\vartheta_{gz}}{\mathrm{d}\tau}\sin 2\vartheta_{gz} + \frac{\mathrm{d}\vartheta_{gz}}{\mathrm{d}\tau}\cos\vartheta_{gz}, \tag{4.61}$$

where

$$b_b = \frac{\eta_b}{I_{gk}\Omega}, \quad b_c = \frac{\eta_c}{I_{gk}\Omega}.$$

If, also in this case, we require that the gyroscope axis must move on the surface of a cone, then programmable controls (4.60) and (4.61) take the following form:

$$M_b(\tau) = \frac{1}{c_b}\Bigg[- \Theta_k \left(\frac{\nu_k}{\Omega}\right)^2 \sin\frac{\nu_k}{\Omega}\tau + b_b\Theta_k \frac{\nu_k}{\Omega}\cos\frac{\nu_k}{\Omega}\tau + \frac{1}{2}\Theta_k^2 \sin^2\frac{\nu_k}{\Omega}\tau \sin 2\left(\Theta_k \sin\frac{\nu_k}{\Omega}\tau\right) - \Theta_k \frac{\nu_k}{\Omega}\sin\frac{\nu_k}{\Omega}\tau \cos\left(\Theta_k \sin\frac{\nu_k}{\Omega}\tau\right)\Bigg], \tag{4.62}$$

$$M_c(\tau) = \frac{1}{c_c}\Bigg[- \Theta_k^2 \left(\frac{\nu_k}{\Omega}\right)^2 \cos\frac{\nu_k}{\Omega}\tau \cos^2\left(\Theta_k \sin\frac{\nu_k}{\Omega}\right) - b_c\Theta_k \frac{\nu_k}{\Omega}\sin\frac{\nu_k}{\Omega}\tau + \frac{1}{2}\Theta_k^2 \left(\frac{\nu_k}{\Omega}\right)^2 \sin 2\frac{\nu_k}{\Omega}\tau \sin 2(\Theta_k \sin p\tau) + \Theta_k \frac{\nu_k}{\Omega}\cos\frac{\nu_k}{\Omega}\tau \cos\left(\Theta_k \sin\frac{\nu_k}{\Omega}\right)\Bigg]. \tag{4.63}$$

The preceding problem of gyroscope axis control on a cone's surface is one of the possible problems. We can substitute other functional relations for the angles $\vartheta_{gz}(\tau)$ and $\psi_{gz}(\tau)$ and their first and second derivatives into the programmable controls governed by (4.60) and (4.61). Some of the most characteristic examples of the required motion of a gyroscope axis that can be applied in detection or tracking systems are depicted below [19, 20]:

1. Motion of gyroscope axis along Archimedes spiral (Fig. 4.3b):

$$\vartheta_{gz}(\tau) = a_g \frac{\nu_s}{\Omega}\tau \sin\left(\frac{\nu_s}{\Omega}\right),$$
$$\psi_{gz}(\tau) = b_g \nu_s \tau \cos\left(\frac{\nu_s}{\Omega}\right). \tag{4.64}$$

2. Motion of gyroscope axis along n-flute rosette (Fig. 4.3c)

$$\vartheta_{gz}(\tau) = \Theta_r \sin\left(\frac{\nu_2}{\Omega}\tau\right)\cos\left(\frac{\nu_1}{\Omega}\tau\right),$$
$$\psi_{gz}(\tau) = \Theta_r \sin\left(\frac{\nu_2}{\Omega}\tau\right)\sin\left(\frac{\nu_1}{\Omega}\tau\right). \tag{4.65}$$

3. Motion of a gyroscope axis along a modified n-flute rosette:

$$\vartheta_{gz}(\tau) = \Theta_r\left[\sin\left(\frac{\nu_2}{\Omega}\tau\right) + 0,2\sin\left(3\frac{\nu_2}{\Omega}\tau\right) + 0.04\sin\left(5\frac{\nu_2}{\Omega}\tau\right)\right]\cos\left(\frac{\nu_1}{\Omega}\tau\right),$$
$$\psi_{gz}(\tau) = \Theta_r\left[\sin\left(\frac{\nu_2}{\Omega}\tau\right) + 0,2\sin\left(3\frac{\nu_2}{\Omega}\tau\right) + 0.04\sin\left(5\frac{\nu_2}{\Omega}\tau\right)\right]\sin\left(\frac{\nu_1}{\Omega}\tau\right). \tag{4.66}$$

4. Motion of gyroscope axis along curve depicted in Fig. 4.3e and described by the following relationships:

$$\vartheta_{gz} = \frac{a_b}{\Omega}\tau\cos\left(\frac{\nu_b}{\Omega}\tau\right) + 0,2a_b\cos\left[2,5\frac{\nu_b}{\Omega}\left(1+\frac{5}{\Omega}\tau\right)\tau\right],$$
$$\psi_{gz} = \frac{a_b}{\Omega}\tau\sin\left(\frac{\nu_b}{\Omega}\tau\right) + 0,2a_b\sin\left[2,5\frac{\nu_b}{\Omega}\left(1+\frac{5}{\Omega}\tau\right)\tau\right]. \tag{4.67}$$

5. Motion of gyroscope axis along curve depicted in Fig. 4.3f and described by the following relationships:

$$\vartheta_{gz} = \begin{cases} 2\pi/(3\Omega)\tau & \text{dla} \quad 0 \le \tau < 0,25\tau_c, \\ -2\pi/(3\Omega)(\tau - 0,5\tau_c) & \text{dla} \quad 0,25\tau_c \le \tau < 0,75\tau_c, \\ 2\pi/(3\Omega)(\tau - \tau_c) & \text{dla} \quad 0,75\tau_c \le \tau < \tau_c, \end{cases}$$
$$\psi_{gz} = a_h\sin\left(\frac{\nu_h}{\Omega}\right); \tag{4.68a}$$

$$\frac{\vartheta_{gz}}{\mathrm{d}\tau} = \begin{cases} 2\pi/(3\Omega) & \text{dla} \quad 0 \le \tau < 0,25\tau_c, \\ -2\pi/(3\Omega) & \text{dla} \quad 0,25\tau_c \le \tau < 0,75\tau_c, \\ 2\pi/(3\Omega) & \text{dla} \quad 0,75\tau_c \le \tau < \tau_c, \end{cases}$$
$$\frac{\psi_{gz}}{\mathrm{d}\tau} = a_h\frac{\nu_h}{\Omega}\cos\left(\frac{\nu_h}{\Omega}\tau\right); \tag{4.68b}$$

$$\frac{\mathrm{d}^2\vartheta_{gz}}{\mathrm{d}\tau^2} = 0, \qquad \frac{\mathrm{d}^2\psi_{gz}}{\mathrm{d}\tau^2} = -a_h\left(\frac{\nu_h}{\Omega}\right)^2\sin\left(\frac{\nu_h}{\Omega}\right). \tag{4.68c}$$

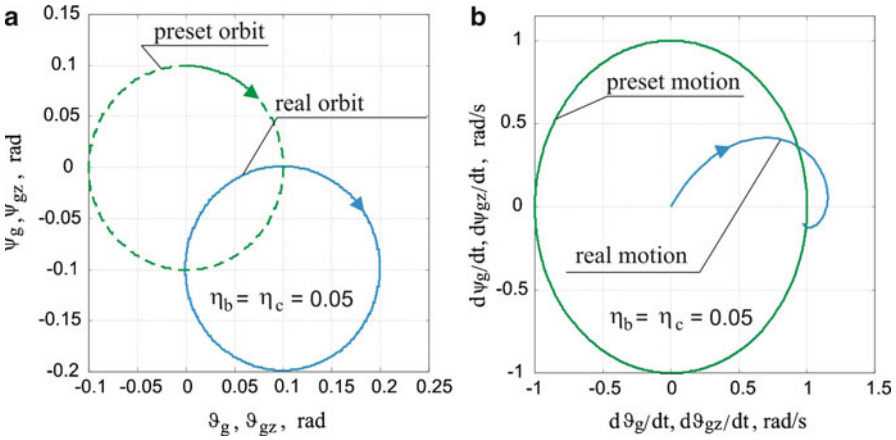

Fig. 4.4 Influence of the initial conditions on realization of motion on the cone surface by the gyroscope axis: (**a**) for angular displacements, (**b**) for angular velocities

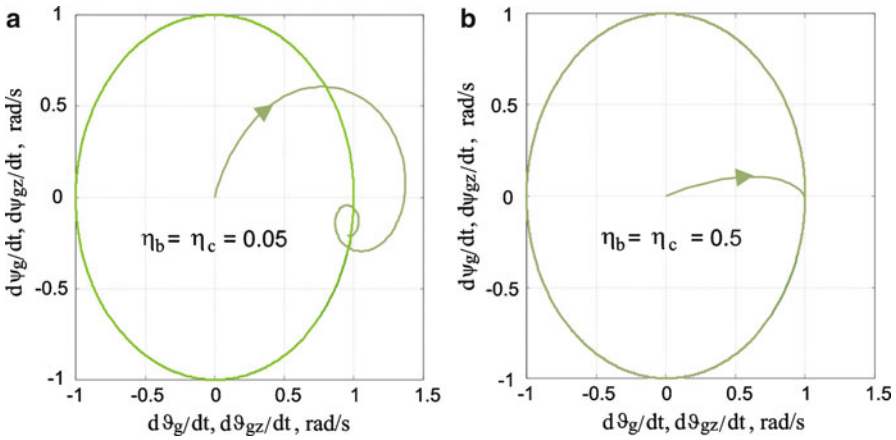

Fig. 4.5 Effect of friction in frame bearings on realization of motion on cone surface by gyroscope axis: (**a**) for small values, (**b**) for large values of viscous damping coefficients

4.2.2 Numerical Example

In Figs. 4.4–4.7, are shown (presented) selected results of computer simulations for two basic motions of a gyroscope axis: (a) describing a cone surface; (b) unfolding the surface after the Archimedes spiral.

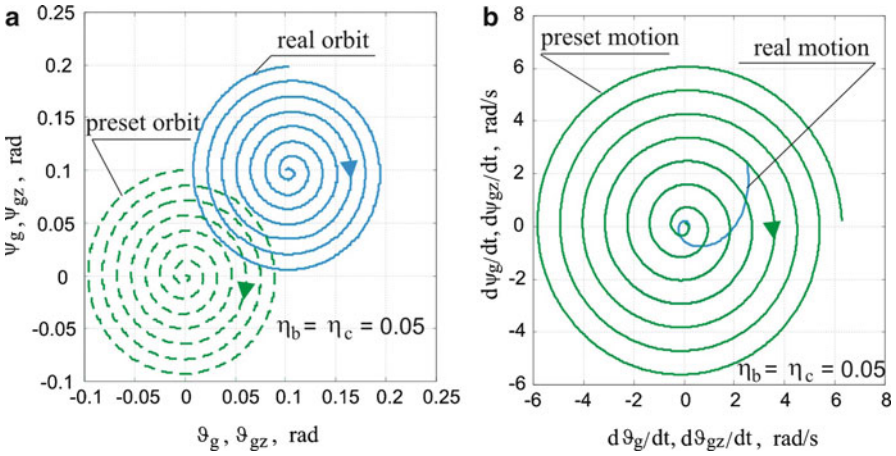

Fig. 4.6 Influence of the initial conditions on realization of the preset motion on the surface described after the Archimede spiral: (**a**) for angular displacements, (**b**) for angular velocities

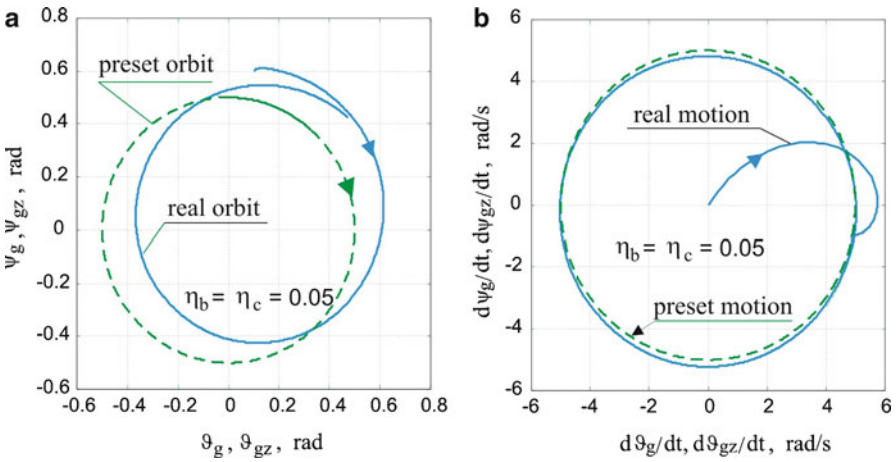

Fig. 4.7 Effect of non-linearities on realization of motion on cone surface by gyroscope axis: (**a**) for angular displacements, (**b**) for angular velocities

Calculations were performed for the following values:

$$I_{go} = 5 \cdot 10^{-4}\text{kgm}^2, \quad I_{gk} = 2.5 \cdot 10^{-4}\text{kgm}^2, \quad \eta_b = \eta_c = 0.1\text{Nms},$$
$$n_g = 600\,\text{rad/s}, \quad \nu_k = 8\,\text{rad/s}, \quad \Omega = 1{,}200\,\text{rad/s}.$$

Figures 4.4 and 4.5 present the negative influence of the initial conditions and coefficients of the friction force η_b, η_c in the frame bearings on the realization of the desired motion. In the initial conditions, unlike in the required ones, $\vartheta_g(0) = -0.1$,

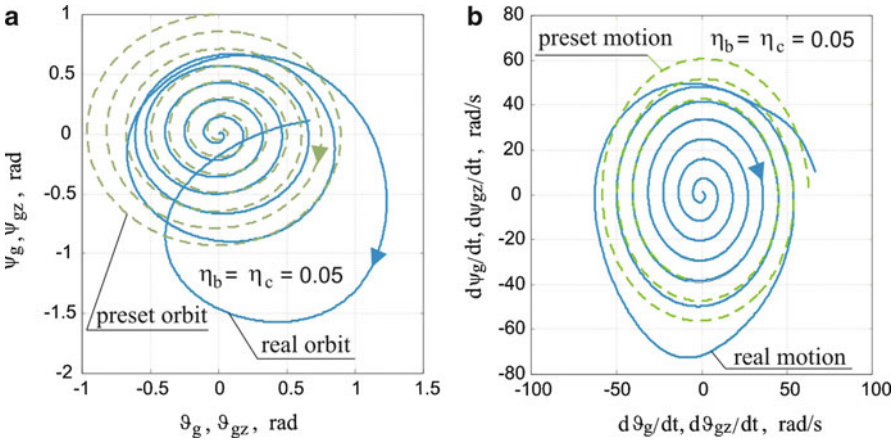

Fig. 4.8 Effect of non-linearities on realization of preset motion on surface described after the Archimedes spiral: (**a**) for angular displacements, (**b**) for angular velocities

$\vartheta_{gz}(0) = 0$, $\psi_g(0) = 0$, $\psi_{gz}(0) = -0.1$, the gyroscope axis does not delineate the required path (Figs. 4.4a and 4.6a), while the angular velocities of the axes are the one we need. However, one can see a transient process (Figs. 4.4b and 4.6b), which is certainly longer at smaller values η_b, η_c and shorter at larger ones (Fig. 4.5a, b).

Figures 4.7 and 4.8 illustrate the effect of large angular displacements on the accuracy of the required motion on the cone surface and along the Archimedes spiral.

4.2.3 Control with Constant Programmable Moments

In order to put a gyroscope axis into a preset path, one needs to change the torques controlling the gyroscope [5, 21]. It is convenient to require to guide, from given initial positions $\vartheta_g(t_0) = \vartheta_{go}$ and $\psi_g(t_0) = \psi_{go}$, the gyroscope axis to the position $\vartheta_{go}(t_0) = \vartheta_{gk}$ and $\psi_{go}(t_0) = \psi_{gk}$ by means of $M_{b_1} = \text{const}$ and $M_{c_1} = \text{const}$. The earlier determined torques M_b and M_c, which we will denote by M_{b_2} and M_{c_2}, will take the gyroscope axis from this position on the preset surface (cone, unfolded along a spiral, rosette, etc.). Thus, we control the gyroscope axis in two stages: in the first stage, the constant moments are applied, and after we reach $\vartheta_g = \vartheta_{go} = \vartheta_{gk}$ and $\psi_g = \psi_{go} = \psi_{gk}$, we go to the second stage, where the moments described by (4.60) and (4.61) are applied.

In the first stage, at the initial conditions $\ddot{\vartheta}_{go} = 0$, $\dot{\vartheta}_{go} = 0$, $\ddot{\psi}_{go} = 0$, $\dot{\psi}_{go} = 0$, we obtain the following solution to (4.56):

$$\vartheta_g(t) = \vartheta_{go} + \frac{\Omega(\eta_c M_{b_1} + M_{c_1})}{I_{gk}\omega_{go}^2}\left[t - \frac{2h_g^*}{\omega_{go}^2}\left(1 - \mathrm{e}^{-h_g^* t}\cos\omega_g^* t\right) - \frac{(\omega_g^*)^2 - (h_g^*)^2}{\omega_{go}^2\omega_g^*}\mathrm{e}^{-h_g^* t}\sin\omega_g^* t\right], \tag{4.69a}$$

$$\psi_g(t) = \vartheta_{go} + \frac{\Omega(\eta_b M_{c_1} - M_{b_1})}{I_{gk}\omega_{go}^2}\left[t - \frac{2h_g^*}{\omega_{go}^2}\left(1 - \mathrm{e}^{-h_g^* t}\cos\omega_g^* t\right) - \frac{(\omega_g^*)^2 - (h_g^*)^2}{\omega_{go}^2\omega_g^*}\mathrm{e}^{-h_g^* t}\sin\omega_g^* t\right], \tag{4.69b}$$

where

$$\omega_g^0 = \sqrt{\omega_{go}^2 - (h_g^*)^2}, \quad \omega_{go}^2 = (1 + \eta_b\eta_c)\Omega^2, \quad h_g^* = \frac{\Omega}{2}(\eta_b + \eta_c).$$

At large values of h_g^* and short time of motion in the first stage, we can make the following approximation:

$$\vartheta_g(t) \approx \vartheta_{go} + \frac{\Omega(\eta_c M_{b_1} + M_{c_1})}{I_{gk}\omega_{go}^2}t, \tag{4.70a}$$

$$\psi_g(t) \approx \psi_{go} + \frac{\Omega(\eta_b M_{c_1} - M_{b_1})}{I_{gk}\omega_{go}^2}t. \tag{4.70b}$$

Now we impose the time during which the axis of the gyroscope travels from the position $\vartheta_{go}, \psi_{go}$ to $\vartheta_g = \vartheta_{gk}, \psi_g = \psi_{gk}$. Let us denote this time by t_u. Then from the preceding equalities (in truth, they are approximated) we obtain

$$\vartheta_{go} + \frac{\Omega(\eta_c M_{b_1} + M_{c_1})}{I_{gk}\omega_{go}^2}t_u = \vartheta_{gk}, \tag{4.71a}$$

$$\psi_{go} + \frac{\Omega(\eta_b M_{c_1} - M_{b_1})}{I_{gk}\omega_{go}^2}t_u = \psi_{gk}. \tag{4.71b}$$

This is a system of two equations with two unknown quantities M_{b_1} and M_{c_1}, and it yields

$$M_{b_1} = -\frac{(\psi_{gk} - \psi_{go} - \eta_b(\vartheta_{gk} - \vartheta_{go}))\cdot I_{go}n_g}{t_u}, \tag{4.72}$$

$$M_{c_1} = \frac{(\vartheta_{gk} - \vartheta_{go} + \eta_c(\psi_{gk} - \psi_{go})) \cdot I_{go} n_g}{t_u}. \tag{4.73}$$

If we want to displace the axis of the gyroscope from the known initial position ϑ_{go}, ψ_{go} to the given position on the surface of the cone $\vartheta_g = \vartheta_{gk}$, $\psi_g = \psi_{gk}$, then the controls have the form

$$M_{b_1} = -\frac{(\psi_{gk} - \psi_{go} + \eta_b \vartheta_{go}) \cdot I_{go} n_g}{t_u}, \tag{4.74a}$$

$$M_{c_1} = \frac{[(\psi_{gk} - \psi_{go})\eta_c - \vartheta_{go}] \cdot I_{go} n_g}{t_u}. \tag{4.74b}$$

When we want to do the same for the preset motion of the axis along the Archimedes spiral, then

$$M_{b_1} = -\frac{(\eta_b \vartheta_{go} - \psi_{go}) \cdot I_{go} n_g}{t_u}, \tag{4.75a}$$

$$M_{c_1} = -\frac{(\eta_c \psi_{go} + \vartheta_{go}) \cdot I_{go} n_g}{t_u}. \tag{4.75b}$$

Summing up, we can say that for the realization of the desired motion, we apply the following algorithm: (1) for $t < t_u$ we control the torques $M_b = M_{b_1}$ and $M_c = M_{c_1}$; (2) for $t \geq t_u$ we control the torques $M_b = M_{b_2}$ and $M_c = M_{c_2}$.

4.2.4 Numerical Example

Figures 4.9 and 4.10 present a process of motion, inconsistent with the preset one, of the gyroscope axis from the initial position to the required one by means of controls M_{b_1}, M_{c_1} described by expressions (4.73). These figures show that a precise realization of the motion of the gyroscope axis is possible along the Archimedes spiral after the gyroscope axis is moved to the required initial position.

4.3 Motion Control of Gyroscope Axis in a Closed System

The results of the preceding section show that programmable control of a gyroscope axis in an open system cannot provide satisfactory accuracy of realization of the preset motion of the axis. The cause are many disturbances, which acts on the gyroscope base.

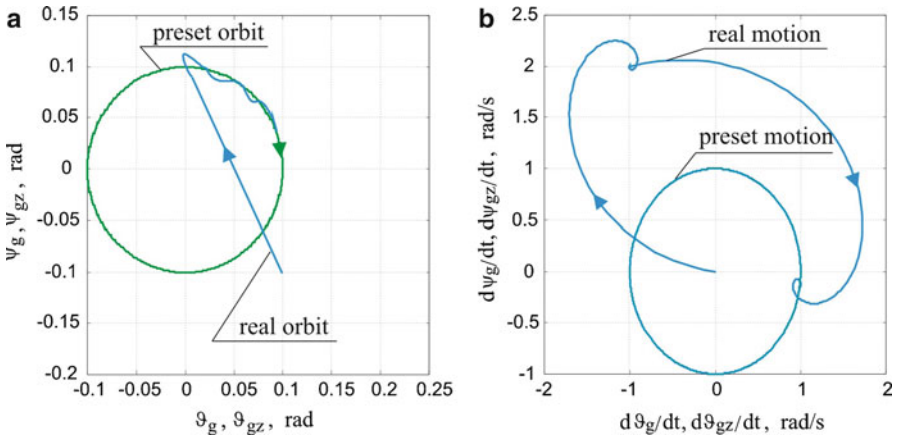

Fig. 4.9 Taking the gyroscope axis to the preset initial position at its motion on the cone surface: (**a**) for angular displacements, (**b**) for angular velocities

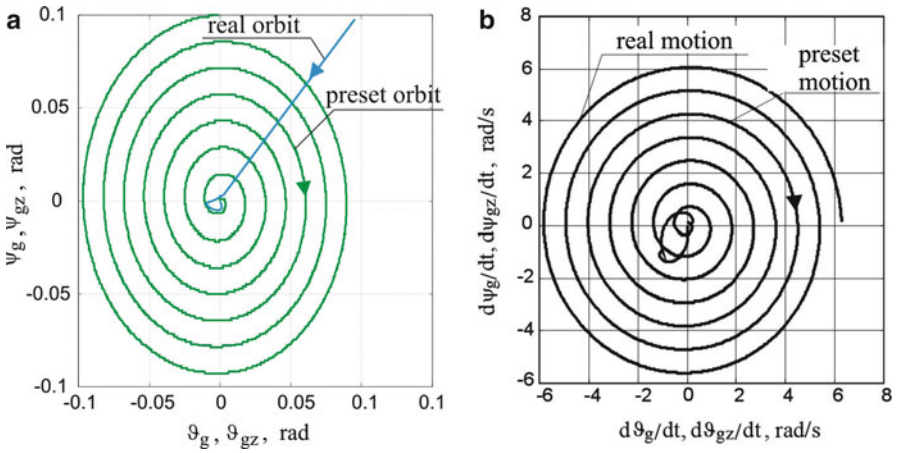

Fig. 4.10 Taking the gyroscope axis to the preset initial position at its motion on the surface, unfolded after the Archimedes spiral: (**a**) for angular displacements, (**b**) for angular velocities

The fundamental elements affecting the errors of not only navigation but also controlled gyroscopes are as follows [22, 23]:

(a) Dry and viscous friction in frame bearings.
(b) Inertia of frames.
(c) Unbalance (static and dynamic) of rotor relative to intersection of frame axes—center of rotation.
(d) Linear and angular accelerations of base.
(e) Elasticity of elements of construction.

(f) Errors of Cardan suspension.
(g) Instability of rotor drive.
(h) Intersection of frames at incorrect angles.
(i) Large angles and angular velocities of deviation of main axis from preset direction.
(j) Rotational motion of Earth.

In order to eliminate the detrimental interaction of the preceding elements one needs to apply systems of automatic correction of the motion of the gyroscope axis.

4.3.1 Gyroscopic System with PID Regulator

Here we will consider control of the gyroscope axis, which relies on tracking, by this axis, a preset direction, which is either time dependent or time independent. The application of such control takes place in various observation instruments, in automatic detection and angular tracking systems, in optical target coordinators of self-guided missiles, etc. [21, 24]. The tracking requires the measurement of the results of control; thus it belongs to the group of *closed control systems* (with feedback) [22]. We will distinguish a *desired* motion (signal) $\vartheta_{gz}(t)$ and $\psi_{gz}(t)$, i.e., the motion of a gyroscope that we would like to realize, and the motion (signal) *realized* $\vartheta_g(t)$ and $\psi_g(t)$ by the gyroscope axis. We will call the deviation of the realized motion from the desired one

$$\Delta_g = \sqrt{(\vartheta_g - \vartheta_{gz})^2 + (\psi_g - \psi_{gz})^2} \tag{4.76}$$

a *real deviation* of the control. Moreover, we will use the notion of *partial deviations*:

$$e_b = \vartheta_g - \vartheta_{gz}, \tag{4.77}$$

$$e_c = \psi_g - \psi_{gz}, \tag{4.78}$$

The basic block diagram of control in a closed system is depicted in Fig. 4.11. Such a scheme of deviation control, in which a *proportional-integral-derivative* (PID) regulator is applied, can serve to control the motion of the gyroscope. Values of the torques M_b and M_c are assumed to be as follows:

$$\begin{aligned} \frac{M_b}{I_{bk}\Omega^2} &= k_b e_b + h_b \frac{\mathrm{d}e_b}{\mathrm{d}t} + h_{b_1} \int_0^t e_b(\tau)\mathrm{d}\tau, \\ \frac{M_c}{I_{bk}\Omega^2} &= k_c e_c + h_c \frac{\mathrm{d}e_c}{\mathrm{d}t} + h_{c_1} \int_0^t e_c(\tau)\mathrm{d}\tau. \end{aligned} \tag{4.79}$$

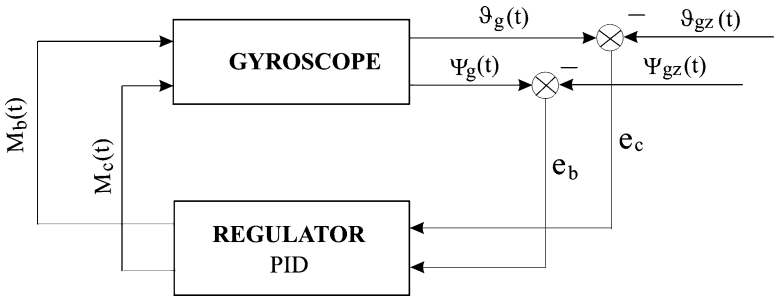

Fig. 4.11 Control scheme in a closed system

One mostly assumes $k_b = k_c, h_b = h_c, h_{b_1} = h_{c_1}$ [22]. However, this is not the most effective control method, which will be shown later in this chapter. The control system should be examined with regard to stability (closed system).

The result of control system operation can be verified by means of a numerical method (computer simulation). For this purpose, we write the linearized equations of motion of gyroscope (4.53), provided that $\vartheta_g << 1$, in the following form:

$$\begin{aligned} I_{gk}\Omega^2\vartheta_g'' + \eta_b\Omega\vartheta_g' - I_{go}n_g\Omega\psi_g' &= M_b, \\ I_{gk}\Omega^2\psi_g'' + \eta_c\Omega\psi_g' + I_{go}n_g\Omega\vartheta_g' &= M_c, \end{aligned} \tag{4.80}$$

or

$$\begin{aligned} \psi_g'' + b_c\psi_g' + \vartheta_g' &= c_c M_c, \\ \vartheta_g'' + b_b\vartheta_g' - \psi_g' &= c_b M_b, \end{aligned} \tag{4.81}$$

where

$$b_b = \frac{\eta_b}{I_{gk}\Omega}, \quad b_c = \frac{\eta_c}{I_{gk}\Omega}, \quad c_b = \frac{1}{I_{gk}\Omega^2}, \quad c_c = \frac{1}{I_{gk}\Omega^2}.$$

Equations of motion of a gyroscope axis in tracking mode are as follows:

$$\vartheta_g'' + b_b\vartheta_g' - \psi_g' = \bar{k}_b(\vartheta_{gz} - \vartheta_g) + \bar{h}_b(\vartheta_{gz}' - \vartheta_g') + \bar{h}_{b_1}\int_0^\tau [\vartheta_{gz}(\tau_1) - \vartheta_g(\tau_1)]\mathrm{d}\tau_1, \tag{4.82a}$$

$$\psi_g'' + b_c\psi_g' + \vartheta_g' = \bar{k}_c(\psi_{gz} - \psi_g) + \bar{h}_c(\psi_{gz}' - \psi_g') + \bar{h}_{c_1}\int_0^\tau [\psi_{gz}(\tau_1) - \psi_g(\tau_1)]\mathrm{d}\tau_1, \tag{4.82b}$$

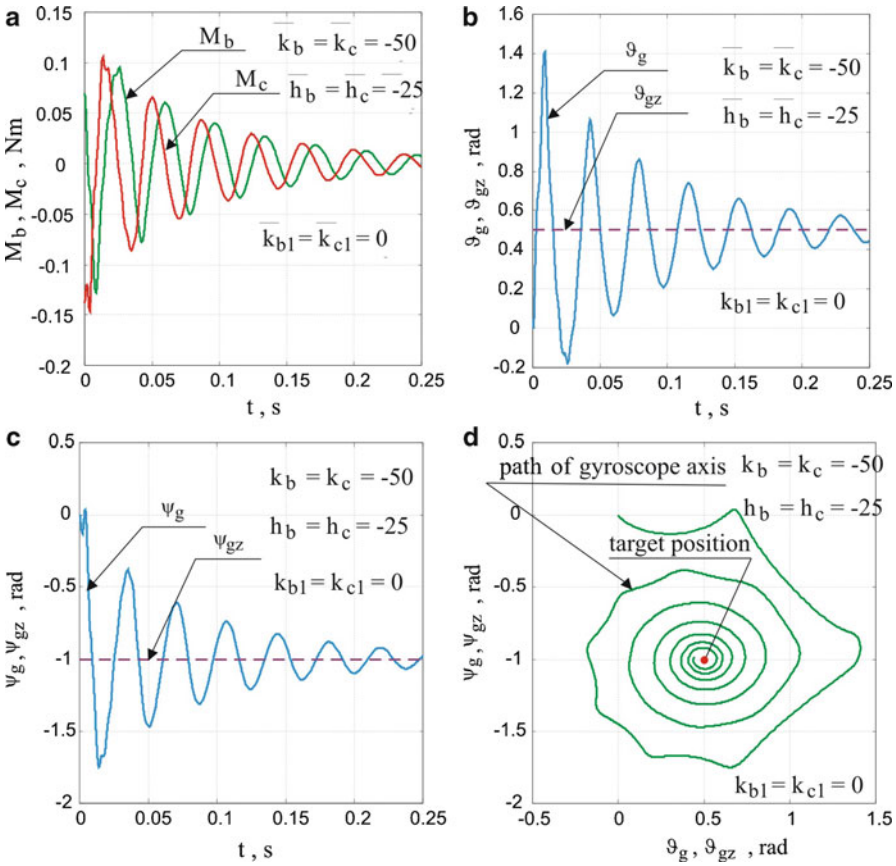

Fig. 4.12 Results of control of gyroscope axis with using PID regulator with small values of damping coefficients at tracking of the fixed point: (**a**) change in control torques as a function of time; (**b, c**) change in angular deviations as a function of time; (**d**) path of gyroscope axis

where

$$\bar{k}_b = \frac{k_b}{I_{gk}\Omega^2}, \quad \bar{k}_c = \frac{k_c}{I_{gk}\Omega^2}, \quad \bar{h}_b = \frac{h_b}{I_{gk}\Omega^2}, \quad \bar{h}_c = \frac{h_c}{I_{gk}\Omega^2}.$$

As a first example, let us examine a procedure for taking a gyroscope axis from the zero position, i.e., $\vartheta_g(0) = 0$, $\dot{\vartheta}_g(0) = 0$, $\psi_g(0) = 0$, and $\dot{\psi}_g(0) = 0$, to the position specified by the angles $\vartheta_g = \vartheta_{c0}$ and $\psi_g = \psi_{c0}$.

Figure 4.12 presents the result of controlling with the use of only a PD-type regulator (without the integrating element $h_{b_1} = h_{c_1} = 0$, $k_b = k_c = -50$, $h_b = h_c = -25$).

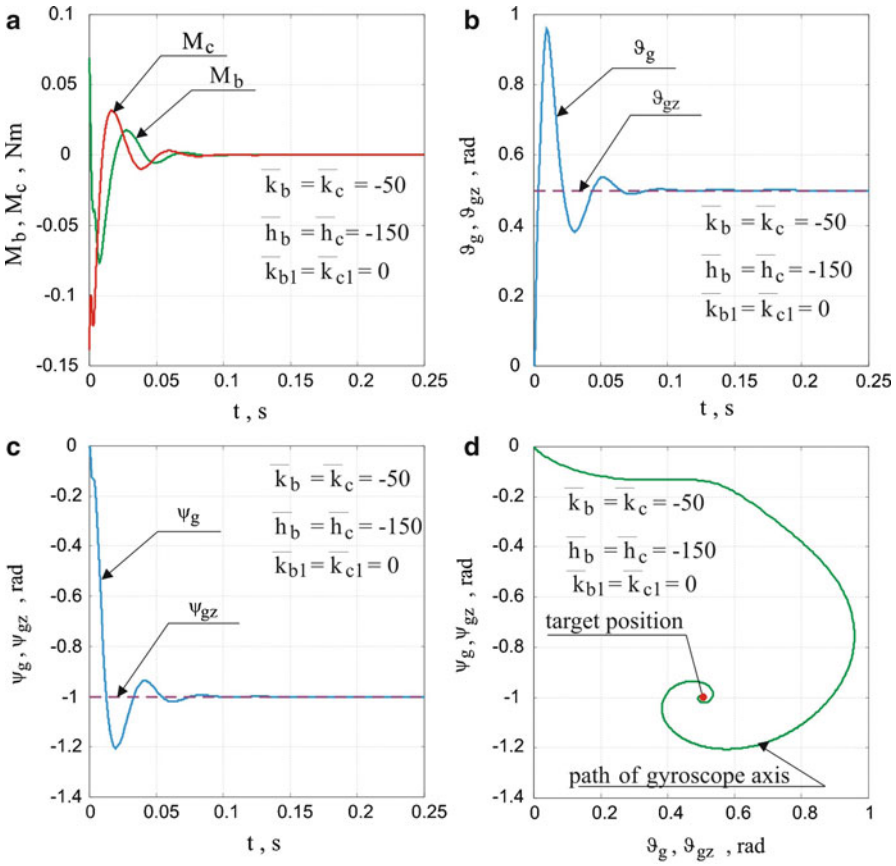

Fig. 4.13 Results of control of gyroscope axis using PID regulator with large values of damping coefficients at tracking of fixed point: (**a**) change of the control torques as a function of time; (**b, c**) change of angular deviations as a function of time; (**d**) path of gyroscope axis

The gyroscope axis makes large displacements, reaching the desired angles over a relatively long time. Increasing values of the damping coefficients $h_b = h_c = -150$ improve this result considerably (Fig. 4.13).

When one selects the regulator parameters $(k_b, k_c, h_b, h_c, h_{b_1}, h_{c_1})$, one needs to check what values the control moments M_b and M_c should be given. In other words, we need to check if these values are not too large to damage the gyroscope. These moments (Fig. 4.12) take on values much larger than those in Fig. 4.13.

The results presented in Figs. 4.12 and 4.13 confirm that a differentiating term, besides a proportional term, plays an important role in the control of a gyroscope axis. The former decides whether regulation is to be realized, whereas the latter increases the damping of system that have a great importance in control of gyroscope. In what follows we will discuss this problem thoroughly. The second

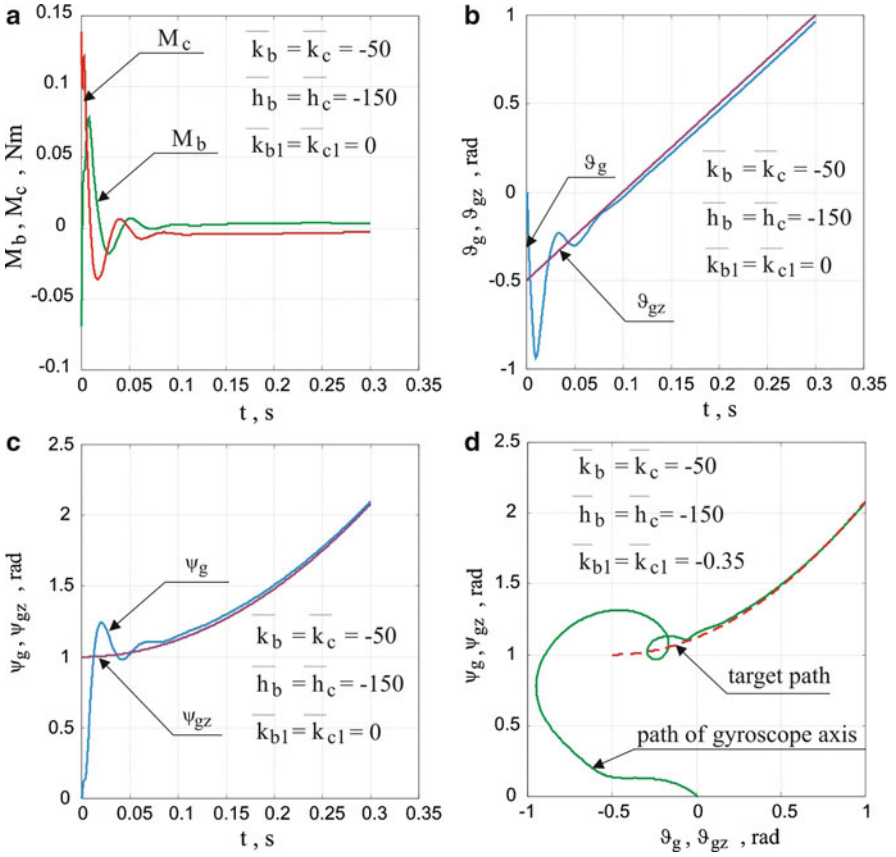

Fig. 4.14 Results of control of gyroscope axis with use of PID regulator with large values of damping coefficients at tracking of movable point: (**a**) change of the control torques as a function of time; (**b, c**) change of angular deviations as a function of time; (**d**) path of gyroscope axis

example covers the tracking of a movable point. The moving point in space is observed from Earth by means of a telescope. The optical axis of the telescope is not coincident with the line connecting this point with the telescope (i.e., the so-called observation line of the target). The telescope objective is located in the gyroscope axis. The problem of control relies on making the axis of the gyroscope coincide with the observation line of the target. Consequently, tracking of the target is performed. In the example, whose results are presented in Figs. 4.14–4.16, a moving point (target) specifies the angles that are required signals according to the following formulas:

$$\vartheta_{gz}(\tau) = \vartheta_{c0} + 0.2 \cdot \omega_c \cdot \tau^2,$$
$$\psi_{gz}(\tau) = \psi_{c0} + \omega_c \cdot \tau.$$

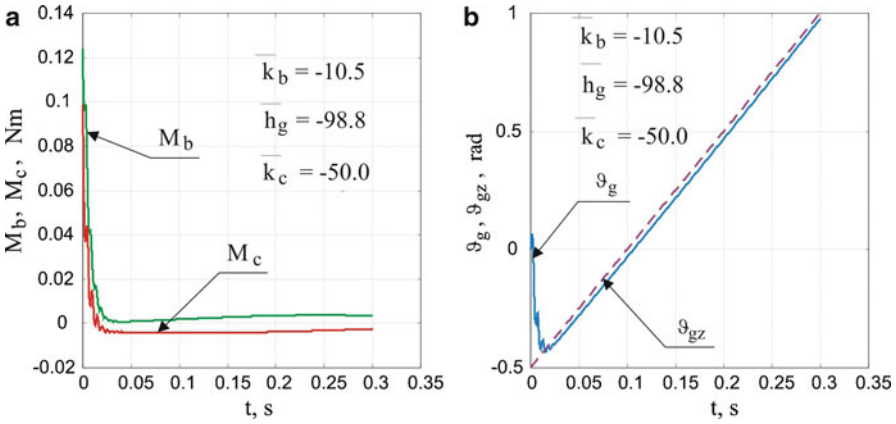

Fig. 4.15 Results of control of gyroscope axis using PID regulator to track fixed point: (**a**) change in control torques as a function of time, (**b**) change in angular deviations as a function of time

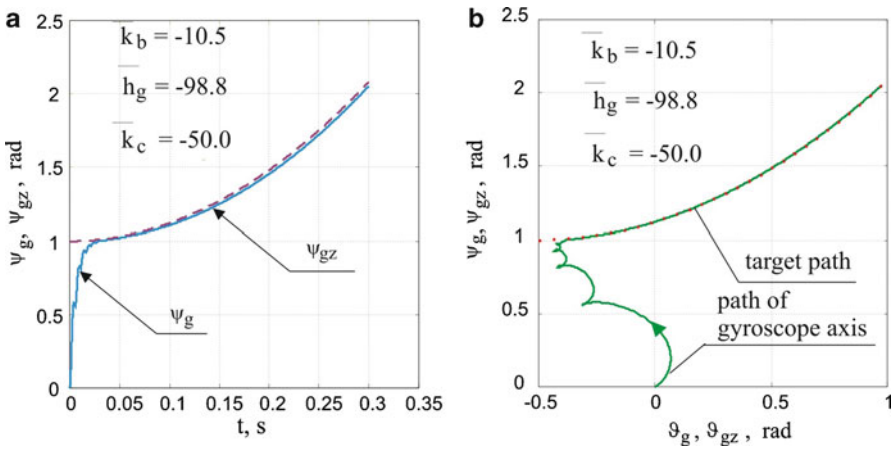

Fig. 4.16 Results of control of gyroscope axis using PID regulator to track movable point: (**a**) change in angular deviations as a function of time, (**b**) path of gyroscope axis

In Fig. 4.14, a regulator without integrating elements leads to the relatively large error Δ_g of the target tracking. Applying a PID-type regulator with specific values of the coefficients improves the tracking (Fig. 4.15).

A more advanced example of gyroscope usage would be a combined method of control of the gyroscope motion. A fixed or movable point in space is to be automatically detected and tracked by an optical system placed in the gyroscope axis, as in the previous examples. The *visual field of the objective* (angle of view) is defined. We have here two states of control of the gyroscope axis. In the first state (seeking the target), the axis "draws" lines in space (e.g., spiral). When the axis approaches the target, so that it is in the vicinity of the objective, a transition

to the second control state occurs. This is a state of target tracking. The axis of the gyroscope approaches the observation line of the target.

4.3.2 Program Control with Feedback

The investigation results mentioned in Sect. 4.1 show that controlling a gyroscope in an open system is saddled with errors caused by the influence of non-linearities. Despite the fact that friction forces in the frame bearings shorten the duration of the transient process, a gyroscope must have those friction forces minimalized. This is implied by the essential task of a gyroscope. Therefore, it is necessary to incorporate a regulator into a gyroscope control system whose role is to minimize errors between the preset and real motions.

In order to determine a program control algorithm with feedback, let us assume that deviations

$$e_b = \vartheta_{gz} - \vartheta_g, \qquad e_c = \psi_{gz} - \psi_g \tag{4.83}$$

change according to the following rules [18]:

$$e_b = C_{b_1} e^{-\lambda_{b_1} t} + C_{b_2} e^{-\lambda_{b_2} t}, \tag{4.84a}$$

$$e_c = C_{c_1} e^{-\lambda_{c_1} t} + C_{c_2} e^{-\lambda_{c_2} t}, \tag{4.84b}$$

which are equivalent to the differential equations

$$\frac{\mathrm{d}^2 e_b}{\mathrm{d}t^2} + (\lambda_{b_1} + \lambda_{b_2}) \frac{\mathrm{d}e_b}{\mathrm{d}t} + \lambda_{b_1} \lambda_{b_2} e_b = 0, \tag{4.85a}$$

$$\frac{\mathrm{d}^2 e_c}{\mathrm{d}t^2} + (\lambda_{c_1} + \lambda_{c_2}) \frac{\mathrm{d}e_c}{\mathrm{d}t} + \lambda_{c_1} \lambda_{c_2} e_c = 0. \tag{4.85b}$$

From (4.85) and (4.84) we have

$$\frac{\mathrm{d}^2 \vartheta_g}{\mathrm{d}t^2} = \frac{\mathrm{d}^2 \vartheta_{gz}}{\mathrm{d}t^2} - (\lambda_{b_1} + \lambda_{b_2}) \frac{\mathrm{d}e_b}{\mathrm{d}t} - \lambda_{b_1} \lambda_{b_2} e_b, \tag{4.86a}$$

$$\frac{\mathrm{d}^2 \psi_g}{\mathrm{d}t^2} \cos^2 \vartheta_g = \left[\frac{\mathrm{d}^2 \psi_{gz}}{\mathrm{d}t^2} - (\lambda_{c_1} + \lambda_{c_2}) \frac{\mathrm{d}e_c}{\mathrm{d}t} - \lambda_{c_1} \lambda_{c_2} e_c \right] \cos^2 \vartheta_g. \tag{4.86b}$$

Substituting the preceding expressions into (4.48) and leaving terms up to the first order of smallness with respect to the deviations e_b and e_c, one obtains the desired control algorithm in a closed system:

$$M_b(t) = M_b^p(t) + u_b(t), \tag{4.87a}$$

$$M_c(t) = M_c^p(t) + u_c(t). \tag{4.87b}$$

The quantities $M_b(t)$ and $M_c(t)$ occurring in (4.87) are program controls of the form

$$M_b^p(t) = I_{gk}\frac{\mathrm{d}^2\vartheta_{gz}}{\mathrm{d}t^2} + \frac{1}{2}I_{gk}\left(\frac{\mathrm{d}\psi_{gz}}{\mathrm{d}t}\right)^2 \sin 2\vartheta_{gz} - I_{go}n_g\frac{\mathrm{d}\psi_{gz}}{\mathrm{d}t}\cos\vartheta_{gz} + \eta_b\frac{\mathrm{d}\vartheta_{gz}}{\mathrm{d}t}, \tag{4.88a}$$

$$M_c^p(t) = I_{gk}\frac{\mathrm{d}^2\psi_{gz}}{\mathrm{d}t^2} - I_{gk}\frac{\mathrm{d}\psi_{gz}}{\mathrm{d}t}\frac{\mathrm{d}\vartheta_{gz}}{\mathrm{d}t}\sin 2\vartheta_{gz} + I_{go}n_g\frac{\mathrm{d}\vartheta_{gz}}{\mathrm{d}t}\cos\vartheta_{gz} + \eta_c\frac{\mathrm{d}\psi_{gz}}{\mathrm{d}t}. \tag{4.88b}$$

The quantities $u_b(t)$ and $u_c(t)$ are correcting controls of the following form:

$$u_b(t) = k_{b_1}(t)\cdot e_b + k_{c_1}(t)\cdot e_c + h_{b_1}(t)\cdot\frac{\mathrm{d}e_b}{\mathrm{d}t} + h_{c_1}(t)\cdot\frac{\mathrm{d}e_c}{\mathrm{d}t}, \tag{4.89a}$$

$$u_c(t) = k_{b_2}(t)\cdot e_b + k_{c_2}(t)\cdot e_b + h_{b_2}(t)\cdot\frac{\mathrm{d}e_b}{\mathrm{d}t} + h_{c_2}(t)\cdot\frac{\mathrm{d}e_c}{\mathrm{d}t}, \tag{4.89b}$$

where

$$k_{b_1}(t) = \frac{1}{2}\left(\frac{\mathrm{d}\psi_{gz}}{\mathrm{d}t}\right)^2\cos 2\vartheta_{gz} + \frac{\psi_{gz}}{\mathrm{d}t}\sin\vartheta_{gz} - \lambda_{b_1}\lambda_{b_2},$$

$$k_{b_2}(t) = \frac{\mathrm{d}\psi_{gz}}{\mathrm{d}t}\frac{\mathrm{d}\vartheta_{gz}}{\mathrm{d}t}\cos 2\vartheta_{gz} + \frac{\vartheta_{gz}}{\mathrm{d}t}\sin\vartheta_{gz},$$

$$k_{c_1}(t) = 0, \qquad k_{c_2}(t) = -\lambda_{c_1}\lambda_{c_2}\cos^2\vartheta_{gz},$$

$$h_{b_1}(t) = -(\eta_b + \lambda_{b_1} + \lambda_{b_2}),$$

$$h_{b_2}(t) = -\left(\frac{\mathrm{d}\psi_{gz}}{\mathrm{d}t}\sin 2\vartheta_{gz} - \cos\vartheta_{gz}\right),$$

$$h_{c_1}(t) = \left(\frac{\mathrm{d}\psi_{gz}}{\mathrm{d}t}\sin 2\vartheta_{gz} - \cos\vartheta_{gz}\right),$$

$$h_{c_2}(t) = -\left[\eta_c + (\lambda_{c_1} + \lambda_{c_2})\cos^2\vartheta_{gz} - \frac{\mathrm{d}\psi_{gz}}{\mathrm{d}t}\sin 2\vartheta_{gz}\right].$$

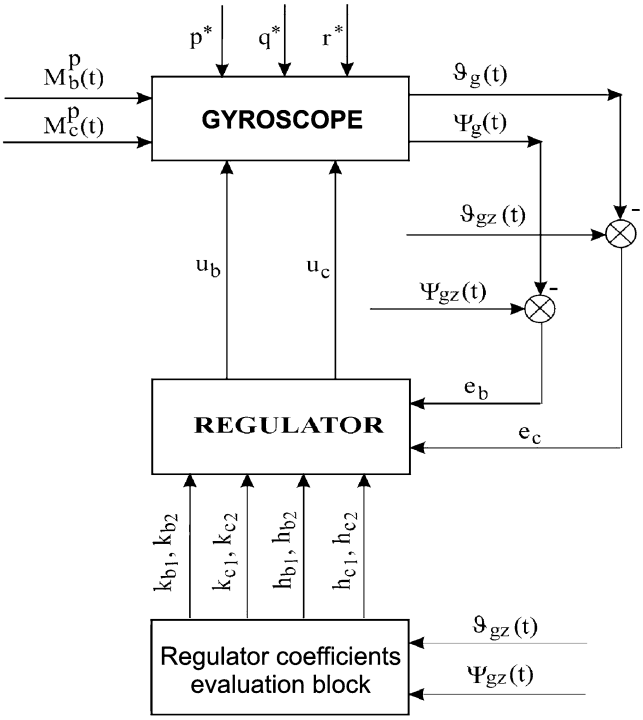

Fig. 4.17 Control scheme of a gyroscope in a closed system

In Fig. 4.17 one can see a functional scheme of the position control of the gyroscope axis in a closed system.

The control algorithm depicted in Fig. 4.17 needs a pre-set change in time of the coefficients of the regulator $k_{b_1}, k_{b_2}, k_{c_2}, h_{b_1}, h_{b_2}, h_{c_1}, h_{c_2}$, which depend on the required values of angular deviations of the gyroscope axis ϑ_{gz}, ψ_{gz} and their first and second derivatives with respect to time. However, one should note that for the quantities ϑ_{gz}, ψ_{gz}, $\frac{d\vartheta_{gz}}{dt}$, $\frac{d\psi_{gz}}{dt}$, $\frac{d^2\vartheta_{gz}}{dt^2}$, $\frac{d^2\psi_{gz}}{dt^2}$ attaining small values we can assume, with a sufficient accuracy from practical viewpoint, constant values of the regulator coefficients, namely,

$$
\begin{aligned}
&k_{b_1} = -\lambda_{b_1}\lambda_{b_2}, \quad k_{b_2} = 0, \quad k_{c_1} = 0, \quad k_{c_2} = -\lambda_{b_1}\lambda_{b_2},\\
&h_{b_1} = -\Big(\eta_b + \lambda_{b_1} + \lambda_{b_2}\Big), \quad h_{c_1} = -I_{go}n_g,\\
&h_{b_2} = I_{go}n_g, \quad h_{c_2} = -\Big(\eta_c + \lambda_{c_1} + \lambda_{c_2}\Big).
\end{aligned}
\tag{4.90}
$$

The quantities λ_{b_1}, λ_{b_2}, λ_{c_1}, λ_{c_2} in (4.90) are constants optimally selected with respect to the minimum of the mean square error and stability of a gyroscope system, which is discussed in the following sections.

4.4 Selection of Optimal Parameters of a Gyroscopic System in Elastic Suspension

In this section, we consider how to select the optimal parameters of a gyroscope whose axis is connected with the rotor by means of an elastic element [16, 18]; this can also be regarded as taking into account the deformability of the rotor construction. It concerns a situation in which the selection of parameters at which the dynamical effects emerging in the transient process will vanish in the shortest time. However, during control of the gyroscope, a sufficient accuracy of the preset position of the gyroscope axis in space can be ensured not just by the gyroscope's construction parameters due to various disturbances. That is why in order to ensure the assumed accuracy of the gyroscope motion, one also needs to select the optimal parameters of the automatic control system of the gyroscope motion. The optimization of the whole gyroscopic system can minimize the dynamical effects. The optimization of parameters is particularly important in the case of scanning of the target coordinator of a self-guided missile or a system for detecting and tracking a target in an unmanned FO (a more detailed discussion is carried out in Chap. 5). In both cases, accuracy is required in the realization of the preset motion and maintenance of the required direction by the gyroscope axis and the fastest damping of transient processes generated from changes in the gyroscope axis motion.

We will consider separately a problem related to the selection of optimal gyroscope parameters and of its automatic control parameters.

4.4.1 Selection of Optimal Parameters of a Gyroscope in Elastic Suspension

The linearized equations of motion (*technical theory*) of a gyroscope in an elastic suspension [derived from (4.31)–(4.35)] are presented in the following form:

$$I^0_{gk}\frac{\mathrm{d}}{\mathrm{d}t}\left(\dot{\vartheta}^0_g+\mathbf{q}^*\right)+\eta_b\dot{\vartheta}^0_g-\kappa\left(\vartheta_g-\vartheta^0_g\right)=M_b, \tag{4.91a}$$

$$I^0_{gk}\frac{\mathrm{d}}{\mathrm{d}t}\left(\dot{\psi}^0_g+\mathbf{r}^*\right)+\eta_c\dot{\psi}^0_g-\kappa\left(\psi_g-\psi^0_g\right)=M_c, \tag{4.91b}$$

$$I_{gk}\frac{\mathrm{d}}{\mathrm{d}t}\left(\dot{\vartheta}_g+\mathbf{q}^*\right)+I_{go}n\left(\dot{\psi}_g+\mathbf{r}^*\right)+\kappa\left(\vartheta_g-\vartheta^0_g\right)=M_{zb}, \tag{4.91c}$$

$$I_{gk}\frac{\mathrm{d}}{\mathrm{d}t}\left(\dot{\psi}_g+\mathbf{r}^*\right)-I_{go}n\left(\dot{\vartheta}_g+\mathbf{q}^*\right)+\kappa\left(\psi_g-\psi^0_g\right)=M_{zc}. \tag{4.91d}$$

Let us apply to the preceding system a dimensionless time

$$\tau = \Omega \cdot t, \tag{4.92a}$$

where

$$\Omega = \frac{I_{go} \cdot n_g}{I_{gk} + I_{gk}^0}. \tag{4.92b}$$

Introducing the independent variable τ (4.92a) and making appropriate transformations, the linearized (4.91) take the following form [15]:

$$\frac{\mathrm{d}^2 \nu_g}{\mathrm{d}\tau^2} = \upsilon_g \frac{\mathrm{d}\sigma_g}{\mathrm{d}\tau} + \upsilon_g \frac{\mathrm{d}\psi_g^0}{\mathrm{d}\tau} + b_b \frac{\mathrm{d}\vartheta_g^0}{\mathrm{d}\tau} - -(\kappa_p + \kappa_0)\nu_g + \bar{M}_{zb} - \bar{M}_b - \mathbf{r}^*, \tag{4.93a}$$

$$\frac{\mathrm{d}^2 \sigma_g}{\mathrm{d}\tau^2} = \upsilon_g \frac{\mathrm{d}\nu_g}{\mathrm{d}\tau} + \upsilon_g \frac{\mathrm{d}\vartheta_g^0}{\mathrm{d}\tau} + b_c \frac{\mathrm{d}\psi_g^0}{\mathrm{d}\tau} - -(\kappa_p + \kappa_0)\sigma_g + \bar{M}_{zc} - \bar{M}_c + \mathbf{q}^*, \tag{4.93b}$$

$$\frac{\mathrm{d}^2 \vartheta_g^0}{\mathrm{d}\tau^2} = -b_b \frac{\mathrm{d}\vartheta_g^0}{\mathrm{d}\tau} + \kappa_0 \nu_g + \bar{M}_b - \frac{\mathrm{d}\mathbf{q}^*}{\mathrm{d}\tau}, \tag{4.93c}$$

$$\frac{\mathrm{d}^2 \psi_g^0}{\mathrm{d}\tau^2} = -b_c \frac{\mathrm{d}\psi_g^0}{\mathrm{d}\tau} + \kappa_0 \sigma_g + \bar{M}_c - \frac{\mathrm{d}\mathbf{r}^*}{\mathrm{d}\tau}, \tag{4.93d}$$

where

$$\nu_g = \vartheta_g - \vartheta_g^0, \quad \sigma_g = \psi_g - \psi_g^0, \quad \upsilon_g = \frac{I_{gk}^0 + I_{gk}}{I_{gk}}, \tag{4.94a}$$

$$b_b = \frac{\eta_b}{I_{gk}^0 \Omega}, \quad b_c = \frac{\eta_c}{I_{gk}^0 \Omega}, \quad \kappa_0 = \frac{\kappa}{I_{gk}^0 \Omega^2}, \quad \kappa_p = \frac{\kappa}{I_{gk}^0 \Omega^2}, \tag{4.94b}$$

$$\bar{M}_b = \frac{M_b}{I_{gk}^0 \Omega^2}, \quad \bar{M}_c = \frac{M_c}{I_{gk}^0 \Omega^2}, \quad \bar{M}_{zb} = \frac{M_{zb}}{I_{gk} \Omega^2}, \quad \bar{M}_{zc} = \frac{M_{zc}}{I_{gk} \Omega^2}.$$

In order to determine stable and optimal parameters we introduce the following designations:

$$\begin{aligned} x_1 &= \nu_g, \qquad x_2 = \frac{\mathrm{d}\nu_g}{\mathrm{d}\tau}, \quad x_3 = \sigma_g, \\ x_4 &= \frac{\mathrm{d}\sigma_g}{\mathrm{d}\tau}, \quad x_5 = \frac{\mathrm{d}\vartheta_g^0}{\mathrm{d}\tau}, \quad x_6 = \frac{\mathrm{d}\psi_g^0}{\mathrm{d}\tau}. \end{aligned} \tag{4.95a}$$

Additionally, let us introduce the following quantities:

$$\bar{b}_b = h_b + b_b, \quad \bar{b}_c = h_c + b_c, \tag{4.95b}$$

where h_b and h_c denote the desired damping needed in the gyroscopic system.

System (4.93), taking into account (4.95), is as follows:

$$\frac{\mathrm{d}\mathbf{x}_g}{\mathrm{d}\tau} = \mathbf{A}_g \mathbf{x}_g, \tag{4.96}$$

where

$$\mathbf{x}_g = [x_1 \quad x_2 \quad x_3 \quad x_4 \quad x_5 \quad x_6]^{\mathrm{T}},$$

$$\mathbf{A}_g = \begin{bmatrix} 0 & 1 & 0 & 0 & 0 & 0 \\ -(\kappa_p + \kappa_0) & 0 & 0 & \upsilon_g & \bar{b}_b & \upsilon_g \\ 0 & 0 & 0 & 1 & 0 & 0 \\ 0 & -\upsilon_g & -(\kappa_p + \kappa_0) & 0 & -\upsilon_g & \bar{b}_c \\ \kappa_0 & 0 & 0 & 0 & -\bar{b}_b & 0 \\ 0 & 0 & \kappa_0 & 0 & 0 & -\bar{b}_c \end{bmatrix}. \tag{4.97}$$

According to the modified Golubientsev method [22, 25], let us introduce a new variable defined as follows:

$$\mathbf{x}_g(\tau) = \mathbf{y}_g(\tau) \cdot e^{\delta_g^*(\tau)}, \tag{4.98}$$

where

$$\delta_g^* = \frac{1}{6}\mathrm{Tr}\mathbf{A}_g = -\frac{1}{6}(\bar{b}_b + \bar{b}_c). \tag{4.99}$$

After some transformations we have

$$\frac{\mathrm{d}\mathbf{y}_g}{\mathrm{d}\tau} = \mathbf{B}_g^* \mathbf{y}_g, \tag{4.100}$$

where

$$\mathbf{B}_g^* = \begin{bmatrix} -\delta_g^* & 1 & 0 & 0 & 0 & 0 \\ -(\kappa_p + \kappa_0) & -\delta_g^* & 0 & \upsilon_g & \bar{b}_b & \upsilon_g \\ 0 & 0 & -\delta_g^* & 1 & 0 & 0 \\ 0 & -\upsilon_g & -(\kappa_p + \kappa_0) & -\delta_g^* & -\upsilon_g & \bar{b}_c \\ \kappa_0 & 0 & 0 & 0 & -\bar{b}_b - \delta_g^* & 0 \\ 0 & 0 & \kappa_0 & 0 & 0 & -\bar{b}_c - \delta_g^* \end{bmatrix}. \tag{4.101}$$

A characteristic equation of matrix $\mathbf{B}_g^*$, whose $\mathrm{Tr}\mathbf{B}_g^* = 0$, is transformed into a characteristic polynomial of the form

$$\lambda_g^6 + b_2\lambda_g^4 - b_3\lambda_g^3 + b_4\lambda_g^2 - b_5\lambda_g + b_6 = 0. \tag{4.102}$$

For matrix $\mathbf{B}_g^*$ we seek values $\kappa_0, \kappa_p, \bar{b}_b, \bar{b}_c$ such that the characteristic (4.102) could possess only imaginary or zero roots [25]. To this end, the coefficients of the characteristic (4.102) b_2, b_3, b_4, b_5, b_6 (coefficient $b_1 = \mathrm{Tr}\mathbf{B}_g^* = 0$) must be determined as sums over all possible combinations of leading-diagonal determinants of degrees 2, 3, 4, 5, and 6 of matrix $\mathbf{B}_g^*$ [(4.101)]. Introducing an additional designation $\bar{\kappa} = (\kappa_0 + \kappa_p)$, we obtain

$$b_2 = -15(\delta_g^*)^2 + 2(\kappa_0 + \kappa_p) + \upsilon_g^2 + \bar{b}_b\bar{b}_c > 0, \tag{4.103}$$

$$b_3 = 40(\delta_g^*)^2 + (2\kappa_p - \kappa_0 + \upsilon_g^2 - 2\bar{b}_b\bar{b}_c)\delta_g^* = 0, \tag{4.104}$$

$$\begin{aligned} b_4 = &-45(\delta_g^*)^2 + 6(\delta_g^*)^2(\bar{b}_b\bar{b}_c - \kappa_0 - 4\kappa_p - 2\upsilon_g^2) \\ &+ 2\kappa_p\bar{b}_b\bar{b}_c + (\bar{b}_b\bar{b}_c + 2\kappa_0)\upsilon_g^2 + (\kappa_0 + \kappa_p)^2 > 0, \end{aligned} \tag{4.105}$$

$$\begin{aligned} b_5 = &24(\delta_g^*)^5 - 2(\delta_g^*)^3(2\bar{b}_b\bar{b}_c - 5\kappa_0 - 14\kappa_p - 7\upsilon_g^2) \\ &- 2\delta_g^*\left[\bar{b}_b\bar{b}_c(2\kappa_p + \upsilon_g^2)\right] + (\kappa_0 + \kappa_p)\cdot(\kappa_0 - 2\kappa_p) - \kappa_0\upsilon_g^2 = 0, \end{aligned} \tag{4.106}$$

$$b_6 = \begin{vmatrix} -\delta_g^* & 1 & 0 & 0 & 0 & 0 \\ -\bar{\kappa} & -\delta_g^* & 0 & \upsilon_g & \bar{b}_b & \upsilon_g \\ 0 & 0 & -\delta_g^* & 1 & 0 & 0 \\ 0 & -\upsilon_g & -\bar{\kappa} & -\delta_g^* & -\upsilon_g & b_c \\ \kappa_0 & 0 & 0 & 0 & -\bar{b}_b - \delta_g^* & 0 \\ 0 & 0 & \kappa_0 & 0 & 0 & -\bar{b}_c - \delta_g^* \end{vmatrix} > 0,$$

$$\begin{aligned} b_6 = &-5(\delta_g^*)^6 + (\delta_g^*)^4(\bar{b}_b\bar{b}_c - 4\kappa_0 - 10\kappa_p - 5\upsilon_g^2) \\ &+ (\delta_g^*)^2\left[\bar{b}_b\bar{b}_c(2\kappa_p + \upsilon_g^2) - 4\kappa_0\upsilon^2 + (\kappa_0 + \kappa_p)(\kappa_0 - 5\kappa_p)\right] \\ &+ \bar{b}_b\bar{b}_c\kappa_p + \kappa_0^2\upsilon_g^2 > 0. \end{aligned} \tag{4.107}$$

Moreover, one needs to take into account a very important condition of absolute maximization of the trace of matrix $\mathbf{A}_g$ defined by (4.97):

$$|\mathrm{Tr}\mathbf{A}_g| = |-(\bar{b}_b + \bar{b}_c)| = \max. \tag{4.108}$$

From the preceding relationships (4.104) and (4.106) for $b_3 = 0$ and $b_5 = 0$ we can determine

$$\kappa_p = \frac{\left[288(\delta_g^*)^2 - 68\bar{b}_b\bar{b}_c + 8\upsilon_g^2(\delta_g^*)^2\right](\delta_g^*)^2 - \bar{b}_b\bar{b}_c\upsilon_g^2 + 4\bar{b}_b^2\bar{b}_c^2}{-36(\delta_g^*)^2 + 4\bar{b}_b\bar{b}_c - \upsilon_g^2}, \tag{4.109a}$$

$$\kappa_0 = 20(\delta_g^*)^2 + \upsilon_g^2 - 2\bar{b}_b\bar{b}_c + 2\kappa_p. \tag{4.109b}$$

From (4.94a) and (4.94b) we have

$$\frac{I_{gk}^0}{I_{gk}} = \frac{\kappa_p}{\kappa_0}, \tag{4.110a}$$

$$\upsilon_g = \frac{\kappa_p}{\kappa_0} + 1, \tag{4.110b}$$

$$\kappa = \frac{\kappa_p}{I_{gk}}\left(\frac{n_g}{\upsilon_g}\right)^2. \tag{4.110c}$$

It follows from (4.110a) that a ratio of transversal moments of inertia of the axis and rotor should equal the ratio of optimal parameters κ_p and κ_0 given in (4.109a) and (4.109b). Formula (4.110c) shows that the coefficient of membrane stiffness κ is directly proportional to the square of the angular velocities of eigenrotations n_g of the gyroscope and inversely proportional to the moment of inertia of the rotor I_{gk}.

Figure 4.18 depicts a scheme of an optimization procedure of linear system parameters of arbitrary dimension. On the basis of the aforementioned scheme, a Matlab Simulink program was created that determines the numerically optimal parameters of the considered dynamical systems.

Figures 4.19 and 4.20 show the dynamical effects of a gyroscope on an elastic suspension excited by the initial conditions. At these optimal parameters (Fig. 4.19) vanishing of the transient process is considerably faster than at parameters that are not optimally selected (Fig. 4.20).

4.4.2 Optimal Control of a Gyroscope in an Elastic Suspension

We will define the law of control of a gyroscope in an elastic suspension by means of the method of linear-square optimization [24, 25] using a functional of the form

$$I = \int_0^\infty \left(\mathbf{x}_g^{\mathrm{T}}\mathbf{Q}_g\mathbf{x}_g + \mathbf{u}_g^{\mathrm{T}}\mathbf{R}_g\mathbf{u}_g\right)\mathrm{d}t. \tag{4.111}$$

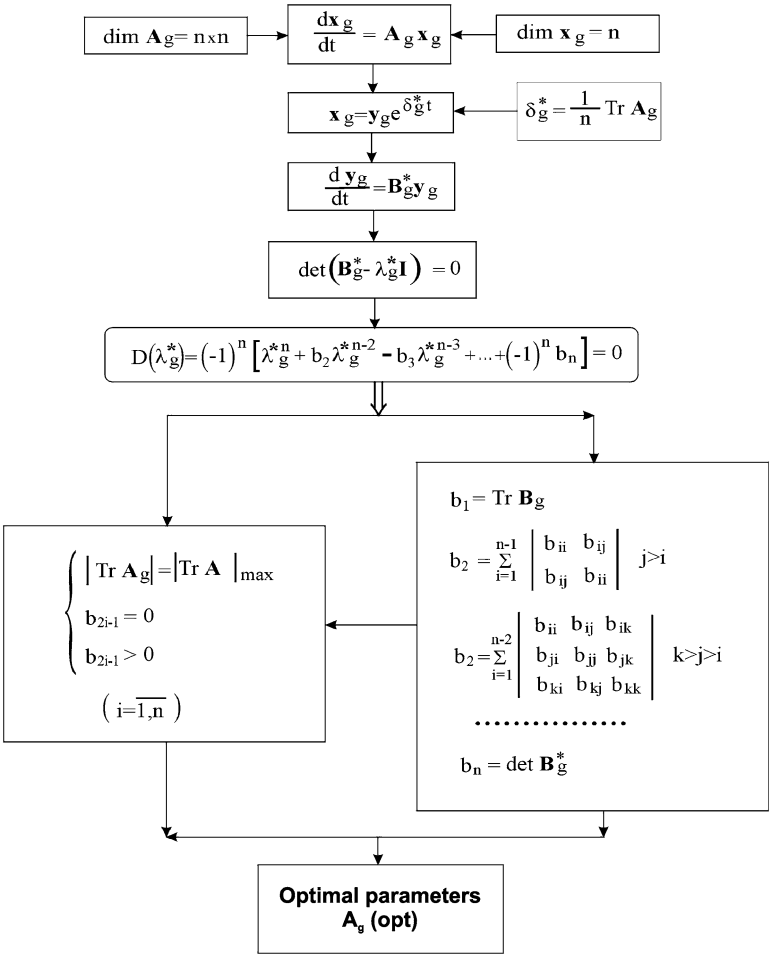

Fig. 4.18 Scheme of optimization of linear system parameters

We will present this law in the following form [23, 24]:

$$\mathbf{u}_g = -\mathbf{K}_g \mathbf{x}_g, \tag{4.112}$$

where

$$\mathbf{u}_g = [U_{zb} \quad U_{zc} \quad U_b \quad U_c]^{\mathrm{T}},$$

$$\mathbf{x}_g = \left[\vartheta_g \quad \frac{\mathrm{d}\vartheta_g}{\mathrm{d}t} \quad \psi_g \quad \frac{\mathrm{d}\psi_g}{\mathrm{d}t} \quad \vartheta_g^0 \quad \frac{\mathrm{d}\vartheta_g^0}{\mathrm{d}t} \quad \psi_g^0 \quad \frac{\mathrm{d}\psi_g^0}{\mathrm{d}t}\right]^{\mathrm{T}}.$$

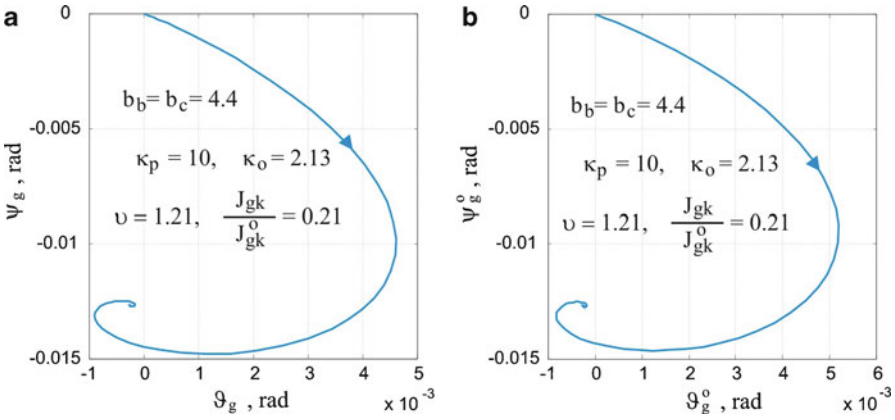

Fig. 4.19 Damping of transient process of optimal gyroscopic system: (**a**) path of gyroscope axis motion, (**b**) motion path of gyroscope axis

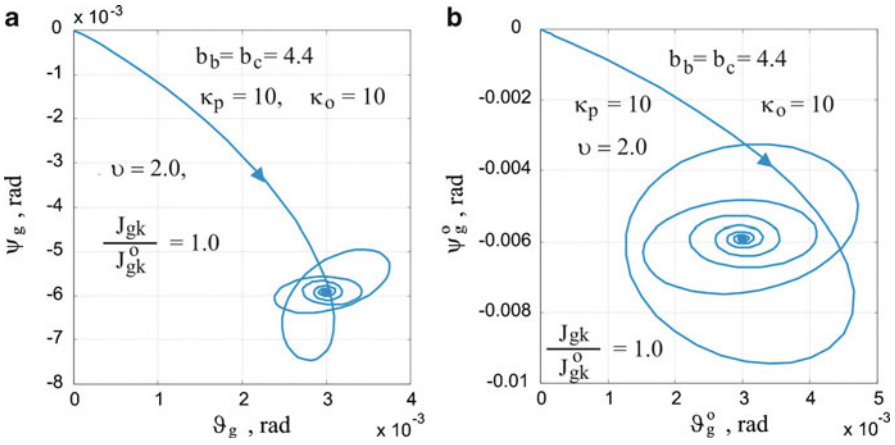

Fig. 4.20 Damping of transient process of non-optimal gyroscopic system: (**a**) motion path of gyroscope rotor axis, (**b**) motion path of gyroscope axis

The coupling matrix $\mathbf{K}_g$ in (4.112) is determined from the following relationship:

$$\mathbf{K}_g = \mathbf{R}_g^{-1}\mathbf{B}_g^{\mathrm{T}}\mathbf{P}_g, \tag{4.113}$$

where

$$\mathbf{B}_g^{\mathrm{T}} = \begin{bmatrix} 0 & c_g & 0 & 0 & 0 & 0 & 0 & 0 \\ 0 & 0 & 0 & c_g & 0 & 0 & 0 & 0 \\ 0 & 0 & 0 & 0 & 0 & c_{go} & 0 & 0 \\ 0 & 0 & 0 & 0 & 0 & 0 & 0 & c_{go} \end{bmatrix}^{\mathrm{T}},$$

$$c_g = \frac{1}{I_{gk}\Omega^2}, \qquad c_{go} = \frac{1}{I^0_{gk}\Omega^2}.$$

Matrix $\mathbf{P}_g$ is a solution of the algebraic Riccati equation

$$\mathbf{A}_g^{\mathrm{T}}\mathbf{P}_g + \mathbf{P}_g\mathbf{A}_g - 2\mathbf{P}_g\mathbf{B}_g\mathbf{R}_g^{-1}\mathbf{B}_g^{\mathrm{T}}\mathbf{P}_g + \mathbf{Q}_g = \mathbf{0}, \tag{4.114a}$$

where $\mathbf{A}_g$ is a state matrix of the form

$$\mathbf{A}_g = \begin{bmatrix} 0 & 1 & 0 & 0 & 0 & 0 & 0 & 0 \\ -\kappa_p & 0 & 0 & -1 & \kappa_p & 0 & 0 & 0 \\ 0 & 0 & 0 & 1 & 0 & 0 & 0 & 0 \\ 0 & 1 & -\kappa_p & 0 & 0 & 0 & \kappa_p & 0 \\ 0 & 0 & 0 & 0 & 0 & 1 & 0 & 0 \\ \kappa_0 & 0 & 0 & 0 & -\kappa_0 & -b_b & 0 & 0 \\ 0 & 0 & 0 & 0 & 0 & 0 & 0 & 1 \\ 0 & 0 & \kappa_0 & 0 & 0 & 0 & -\kappa_0 & -b_c \end{bmatrix}. \tag{4.114b}$$

The weight matrices $\mathbf{R}_g$ and $\mathbf{Q}_g$ in (4.113) and (4.114a), transformed into diagonal forms, are selected experimentally, where the search is initiated from the following values [22]:

$$q_{ii} = \frac{1}{2x_{i_{\max}}}, \qquad r_{ii} = \frac{1}{2u_{i_{\max}}}, \qquad (i = 1, 2, \ldots, 8), \tag{4.115}$$

where $x_{i_{\max}}$ is the maximal range of change of the ith value of the state variable, $u_{i_{\max}}$ is the maximal range of change of the ith value of the control variable.

Solving numerically the matrix Ricatti (4.114a) and determining the gain matrix $\mathbf{K}_g$, one can observe that for the analyzed case, particular elements of the matrix satisfy the following relationships:

$$k_{11} = k_{23} = k_{z_\vartheta}, \qquad k_{12} = k_{24} = h_{z_\vartheta}, \qquad k_{13} = -k_{21} = k_{z_\psi},$$

$$k_{14} = k_{22} = h_{z_\psi} = 0, \qquad k_{15} = k_{27} = k_{z_{\vartheta_0}}, \qquad k_{16} = -k_{28} = h_{z_{\vartheta_0}},$$

$$k_{17} = k_{25} = k_{z_{\psi_0}}, \qquad k_{18} = -k_{26} = h_{z_{\psi_0}}, \qquad k_{31} = k_{43} = k_\vartheta,$$

$$k_{32} = k_{44} = h_\vartheta, \qquad k_{33} = -k_{41} = k_\psi, \qquad k_{34} = -k_{42} = h_\psi,$$

$$k_{35} = k_{47} = k_{\vartheta_0}, \qquad k_{36} = k_{48} = h_{\vartheta_0}, \qquad k_{37} = -k_{45} = k_{\psi_0},$$

$$k_{38} = k_{46} = h_{\psi_0} = 0.$$

It follows from the preceding relationships and (4.112) that the control torques influencing the gyroscope will have the form

$$U_{zb} = -k_{z_\vartheta}\vartheta_g - h_{z_\vartheta}\frac{\mathrm{d}\vartheta_g}{\mathrm{d}\tau} + k_{z_\psi}\psi_g - k_{z_{\vartheta_0}}\vartheta_g^0 + h_{z_{\vartheta_0}}\frac{\mathrm{d}\vartheta_g^0}{\mathrm{d}\tau} - k_{z_{\psi_0}}\psi_g^0 + h_{z\psi_0}\frac{\mathrm{d}\psi_g^0}{\mathrm{d}\tau}, \tag{4.116}$$

$$U_{zc} = -k_{z_\psi}\vartheta_g - h_{z_\vartheta}\frac{\mathrm{d}\psi_g}{\mathrm{d}\tau} - k_{z_\vartheta}\psi_g - k_{z_{\psi_0}}\vartheta_g^0 - h_{z_{\psi_0}}\frac{\mathrm{d}\vartheta_g^0}{\mathrm{d}\tau} - k_{z_{\vartheta_0}}\psi_g^0 - h_{z\vartheta_0}\frac{\mathrm{d}\psi_g^0}{\mathrm{d}\tau}, \tag{4.117}$$

$$U_b = -k_\vartheta\vartheta_g - h_\vartheta\frac{\mathrm{d}\vartheta_g}{\mathrm{d}\tau} - k_\psi\psi_g + h_\psi\frac{\mathrm{d}\psi_g}{\mathrm{d}\tau} - k_{\vartheta_0}\vartheta_g^0 - h_{\vartheta_0}\frac{\mathrm{d}\vartheta_g^0}{\mathrm{d}\tau} + k_{\psi_0}\psi_g^0, \tag{4.118}$$

$$U_c = -k_\psi\vartheta_g - h_\psi\frac{\mathrm{d}\vartheta_g}{\mathrm{d}\tau} - k_\vartheta\psi_g - h_\vartheta\frac{\mathrm{d}\psi_g}{\mathrm{d}\tau} - k_{\psi_0}\vartheta_g^0 - h_{\vartheta_0}\frac{\mathrm{d}\psi_g^0}{\mathrm{d}\tau} - k_{\vartheta_0}\psi_g^0. \tag{4.119}$$

Applying the preceding controls to the gyroscope described by (4.96), we obtain a new gyroscopic system of the form

$$\frac{\mathrm{d}\mathbf{x}_g}{\mathrm{d}\tau} = \mathbf{A}_g^*\mathbf{x}_g, \tag{4.120}$$

where

$$\mathbf{A}_g^* = \mathbf{A}_g - \mathbf{B}_g\mathbf{R}_g^{-1}\mathbf{B}_g^{\mathrm{T}}\mathbf{P}_g.$$

System (4.120) can be optimized according to the algorithm depicted in Fig. 4.18. The additional optimization by means of the modified Golubientsev method can be carried out if the gyroscopic system (4.120) is to be applied in devices of target detection and tracking systems [21]. This concerns the minimization of the transient process duration at the moment of target detection, which holds great significance for the maintenance of this target near the tracking system [22, 25].

A block diagram of the algorithm of a linear-square optimization, along with the modified Golubientsev method of any control system, is presented in Fig. 4.21.

4.4.3 Results of Digital Investigations

The results of controlling a gyroscope suspended in an elastic suspension are depicted in Figs. 4.22–4.26. A control problem depends on putting the gyroscope axis in the pre-set motion, in which the gyroscope axis moves on a cone surface

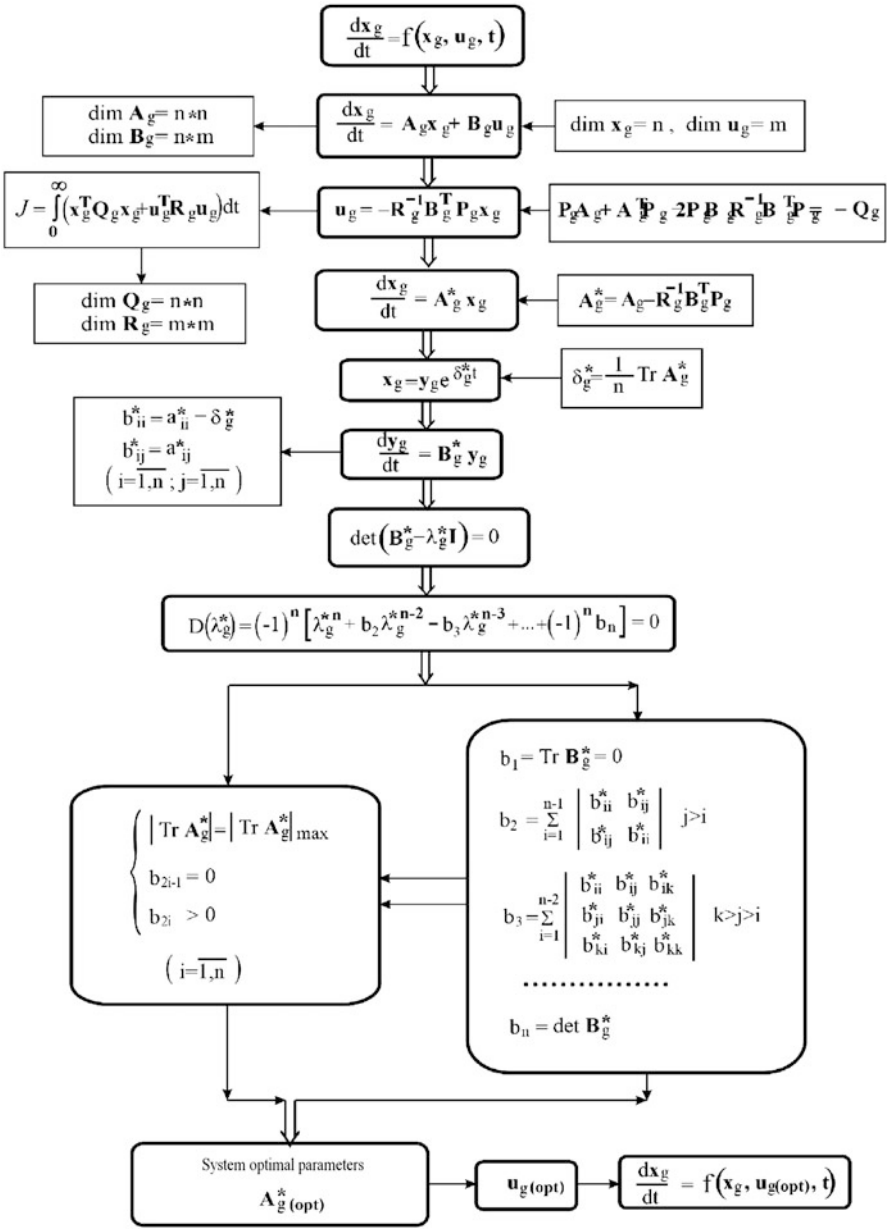

Fig. 4.21 Block diagram of complete system optimization

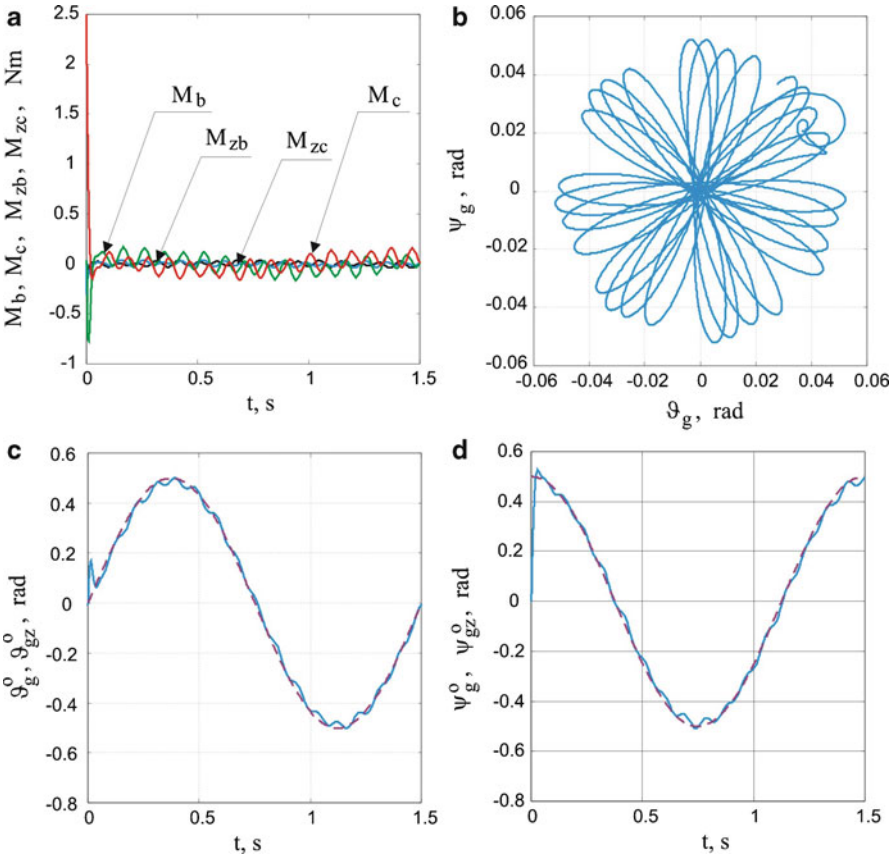

Fig. 4.22 Gyroscope control in elastic suspension using PID regulator: (**a**) change in control torques as a function of time, (**b**) path of gyroscope axis, (**c**), (**d**) change in preset and realized angular deviations of gyroscope axis as a function of time

(Figs. 4.22–4.24) or on an Archimedes spiral (Figs. 4.25 and 4.26), and the rotor axis plots n-flute rosette. For all of the cases the gyroscope parameters are the same as in Sect. 4.2. Figures 4.22 and 4.23 present the behavior of a gyroscope with the PID regulator applied, with non-optimal coefficients.

In Fig. 4.24 one can observe an essential improvement in realization of motion, preset by the gyroscope after introduction of controls, selected on the basis of the algorithm illustrated in Fig. 4.21. The efficiency of the optimal control is depicted in Fig. 4.25, where, despite the action of the impulse of torque, the preset motion is instantiated. We have a similar situation in the case of the effect of kinematic excitations on gyroscope suspension in the form of harmonic vibrations.

We applied optimal gain coefficients of the control torques described by relationships (4.117)–(4.120) with the following values:

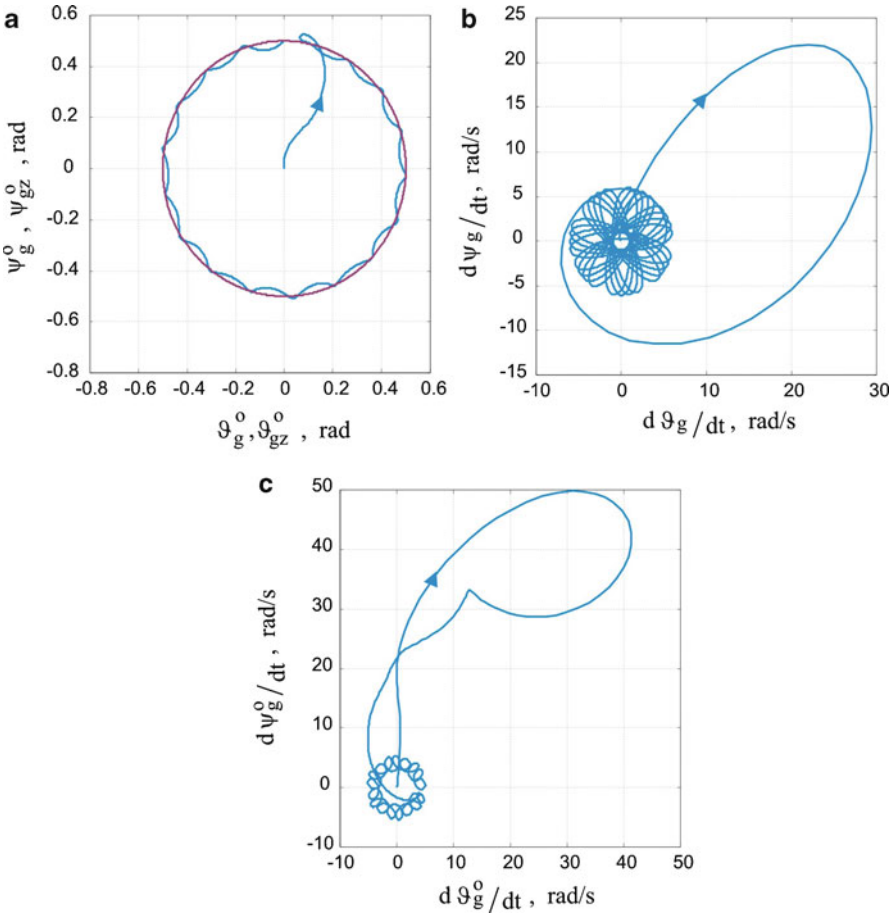

Fig. 4.23 Gyroscope control in elastic suspension using PID regulator: (**a**) preset and realized path of gyroscope axis, (**b**) angular velocities of rotor axis of gyroscope in phase plane, (**c**) angular velocities of gyroscope axis in phase plane

$$k_{z\vartheta} = -0.0155, \quad h_{z\vartheta} = 73.67, \quad k_{z\psi} = -0.355, \quad h_{z\psi} = 0.00,$$

$$k_{z\vartheta_0} = 0.477, \quad h_{z\vartheta_0} = 0.756, \quad k_{z\psi_0} = -0.471, \quad h_{z\psi} = -0.0146,$$

$$k_{\vartheta} = -0.128, \quad h_{\vartheta} = 3.549, \quad k_{\psi} = -2.125, \quad h_{\psi} = 0.0686,$$

$$k_{\vartheta_0} = 12.574, \quad h_{\vartheta_0} = 20.898, \quad k_{\psi_0} = -2.633, \quad h_{\psi_0} = 0.00.$$

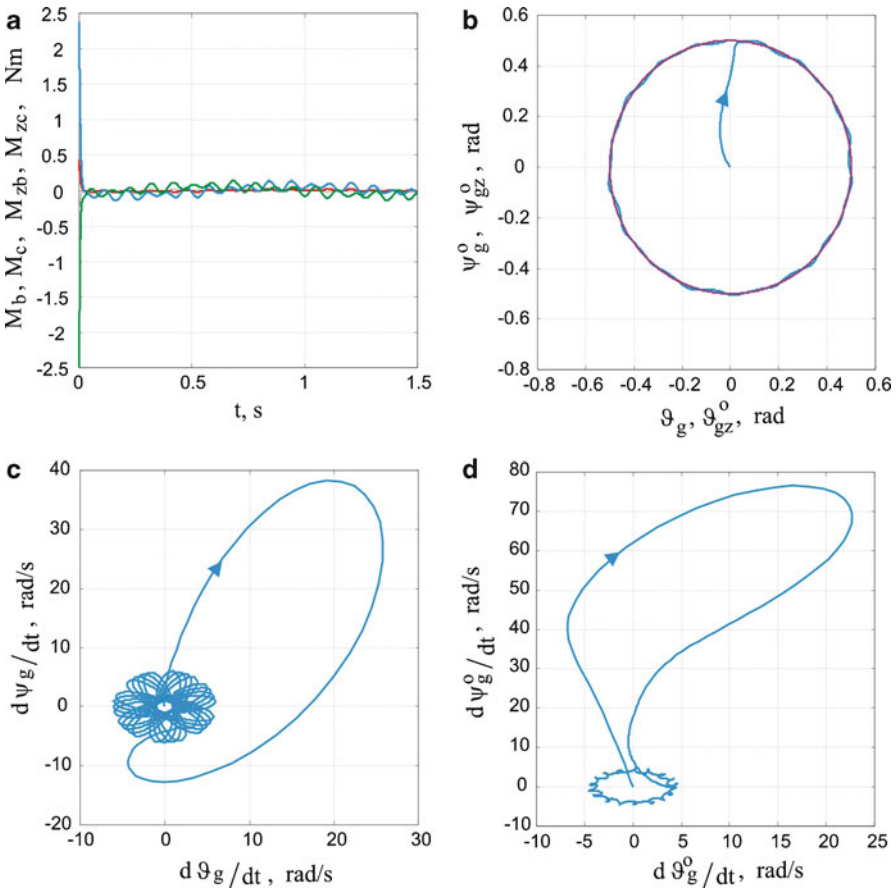

Fig. 4.24 Gyroscope control in elastic suspension using optimal control torques: (**a**) change in control torques as a function of time, (**b**) preset and realized path of gyroscope axis, (**c**) angular velocities of rotor axis of gyroscope in phase plane, (**d**) angular velocities of gyroscope axis in phase plane

4.5 Selection of Optimal Parameters of a Gyroscopic System with an Axis Fixed to Rotor

4.5.1 Optimization of a Classic Controlled Gyroscope

The linearized model of a controlled gyroscopic system with an axis permanently connected to a rotor is presented as follows

$$\frac{d\mathbf{x}_g}{d\tau} = \mathbf{A}_g\mathbf{x}_g + \mathbf{B}_g\mathbf{u}_g, \tag{4.121}$$

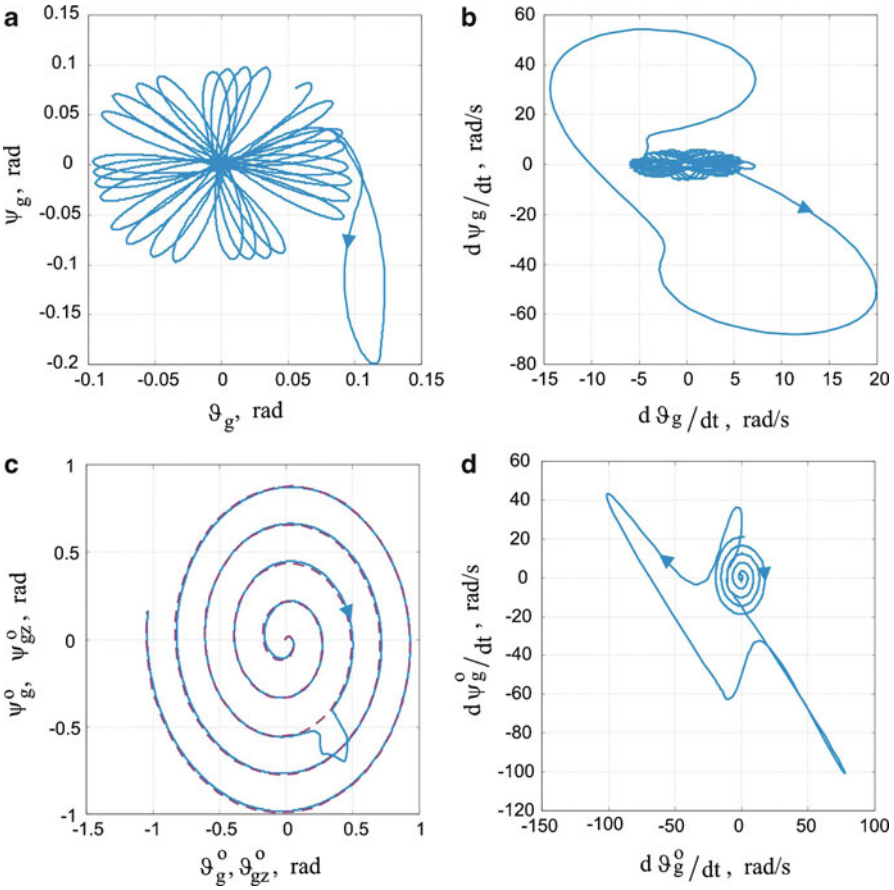

Fig. 4.25 Gyroscope control in elastic suspension using optimal control torques under action of impulse of pair of forces: (**a**) path of rotor axis of gyroscope, (**b**) angular velocities of rotor axis of gyroscope in phase plane, (**c**) preset and realized path of gyroscope axis, (**d**) angular velocities of gyroscope axis in phase plane

where

$$\mathbf{x}_g = \left[\vartheta_g \quad \frac{\mathrm{d}\vartheta_g}{\mathrm{d}\tau} \quad \psi_g \quad \frac{\mathrm{d}\psi_g}{\mathrm{d}\tau}\right]^{\mathrm{T}}, \qquad \mathbf{u}_g = [u_b \quad u_c]^{\mathrm{T}},$$

$$\mathbf{A}_g = \begin{bmatrix} 0 & 1 & 0 & 0 \\ 0 & -b_b & 0 & -1 \\ 0 & 0 & 0 & 1 \\ 0 & 1 & 0 & -b_c \end{bmatrix}, \qquad \mathbf{B}_g = \begin{bmatrix} 0 & 0 \\ c_b & 0 \\ 0 & 0 \\ 0 & c_c \end{bmatrix}.$$

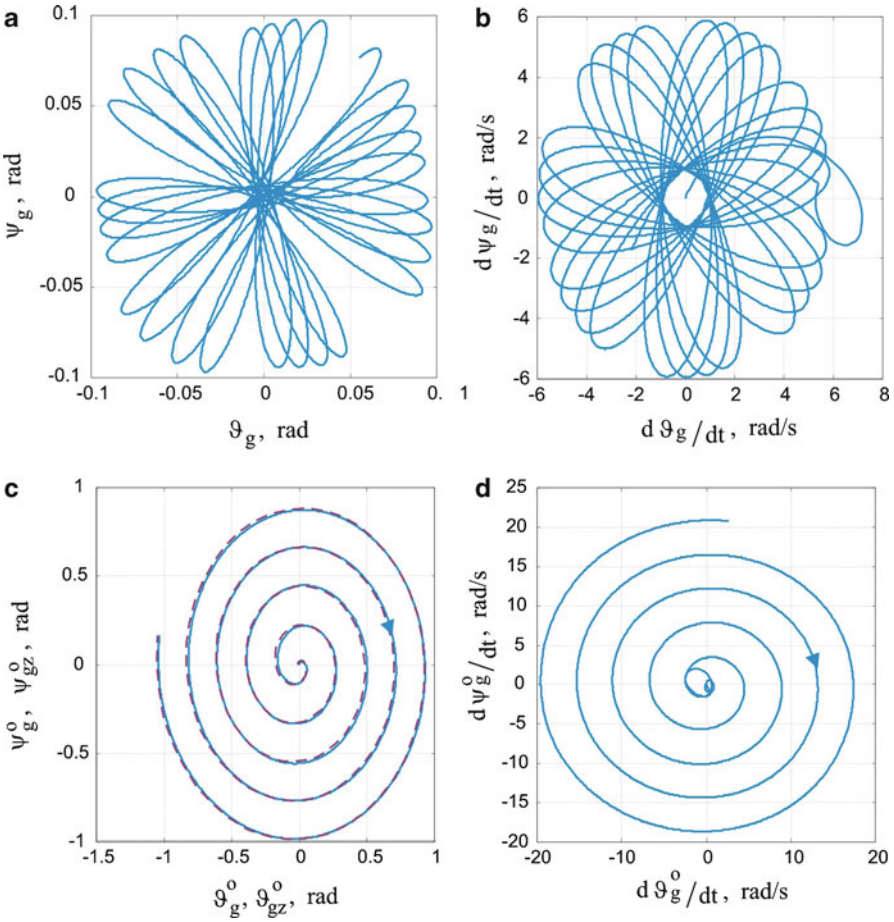

Fig. 4.26 Controlling a gyroscope suspended in an elastic suspension using optimal control torques under action of kinematic excitements of base: (**a**) path of rotor axis, (**b**) angular velocities of rotor axis in phase plane, (**c**) preset and realized path of gyroscope axis, (**d**) angular velocities of gyroscope axes in phase plane

In order to ensure that the controlled gyroscope governed by (4.121) has stability and a shortest transient process, as in the preceding section, we will introduce an optimal control of the form

$$\mathbf{u}_g = -\mathbf{K}_g \mathbf{x}_g, \tag{4.122}$$

where

$$\mathbf{K}_g = \begin{bmatrix} k_{11} & k_{12} & k_{13} & k_{14} \\ k_{21} & k_{22} & k_{23} & k_{24} \end{bmatrix}.$$

Similarly to the case of the gyroscopic system in an elastic suspension described by state matrix (4.114a), the particular elements of gain matrix $\mathbf{K}_g$ satisfy the following relationships for the analyzed case:

$$\begin{aligned} k_{11} &= k_{23} = \bar{k}_b, \\ k_{12} &= k_{14} = k_{22} = k_{24} = \bar{h}_g, \\ k_{21} &= -k_{13} = \bar{k}_c. \end{aligned} \tag{4.123}$$

Substituting the gain coefficients (4.123) into (4.122), the correcting controls take the form

$$u_b = -\bar{k}_b \vartheta_g + \bar{k}_c \psi_g - \bar{h}_g \frac{\mathrm{d}\vartheta_g}{\mathrm{d}\tau}, \tag{4.124a}$$

$$u_c = -\bar{k}_c \vartheta_g - \bar{k}_b \psi_g - \bar{h}_g \frac{\mathrm{d}\psi_g}{\mathrm{d}\tau}, \tag{4.124b}$$

where

$$\bar{k}_b = \frac{k_b}{I_{gk}\Omega^2}, \quad \bar{k}_c = \frac{k_c}{I_{gk}\Omega^2}, \quad \bar{h}_g = \frac{h_g}{I_{gk}\Omega}. \tag{4.125}$$

Thus, the gyroscopic system in the closed system (4.121), including (4.124), is reduced to a new form:

$$\frac{\mathrm{d}\mathbf{x}_g}{\mathrm{d}\tau} = \mathbf{A}_g^* \mathbf{x}_g, \tag{4.126}$$

where

$$\mathbf{A}_g^* = \begin{bmatrix} 0 & 1 & 0 & 0 \\ -\bar{k}_b & -\bar{h}_g - b_b & \bar{k}_c & 1 \\ 0 & 0 & 0 & 1 \\ -\bar{k}_c & -1 & -\bar{k}_b & -\bar{h}_g - b_c \end{bmatrix}. \tag{4.127}$$

Henceforth, we will assume that friction in the suspension bearings is negligible, i.e., $b_b = b_c = 0$. For a gyroscopic system like this, we will seek two more parameters and relations between them for which the duration of the transient process damping is the shortest. In this case, we will also apply the modified optimization method of Golubientsev, whose algorithm is presented in Fig. 4.18.

We obtain the following system of equations and inequalities from the stability conditions of Hurwitz and modified Golubientsev optimization method [25]:

$$\bar{k}_b > 0, \quad \bar{k}_c > 0, \quad \bar{h}_g > 0, \tag{4.128}$$

$$2\bar{k}_b - \frac{1}{2}\bar{h}_g^2 + 1 > 0, \tag{4.129}$$

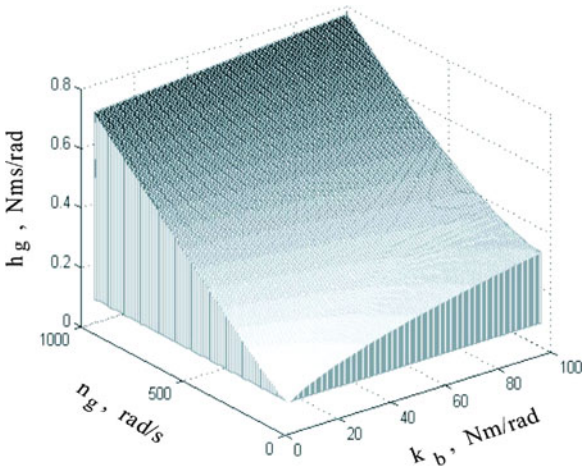

Fig. 4.27 Graph of mutually optimal relations of damping coefficient of regulator h_g, angular velocity n_g, and gain factor k_b

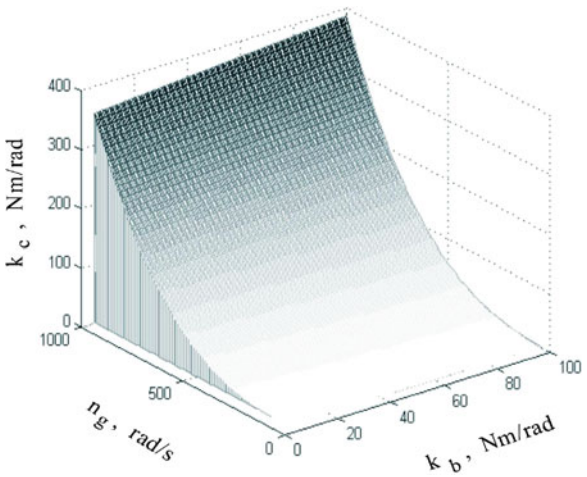

Fig. 4.28 Graph of mutual optimal relationships of gain coefficient of regulator k_c, angular velocity n_g, and gain coefficient k_b

$$\bar{k}_c = \frac{1}{2}\bar{h}_g, \tag{4.130}$$

$$\frac{1}{16}\bar{h}_g^4 + \frac{1}{4}\bar{h}_g^2 - \frac{1}{2}\bar{h}_g^2\bar{k}_b - \bar{h}_g\bar{k}_c + \bar{k}_b^2 + \bar{k}_c^2 > 0. \tag{4.131}$$

Taking into account the condition of maximization of absolute value of a trace of matrix $\mathbf{A}_g^*$ yields

$$|\mathrm{Tr}\mathbf{A}_g^*| \to \max. \tag{4.132}$$

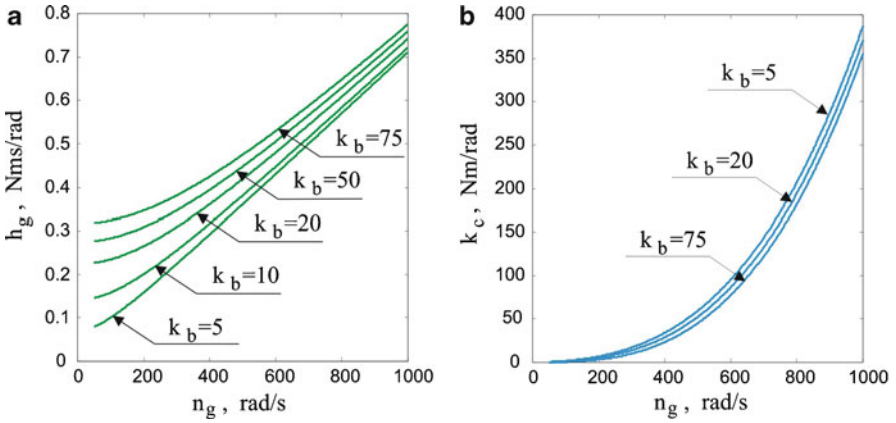

Fig. 4.29 Graph of optimal relationships of regulator coefficients (**a**) h_g, (**b**) k_c vs. angular velocity n_g at different gain coefficient k_b

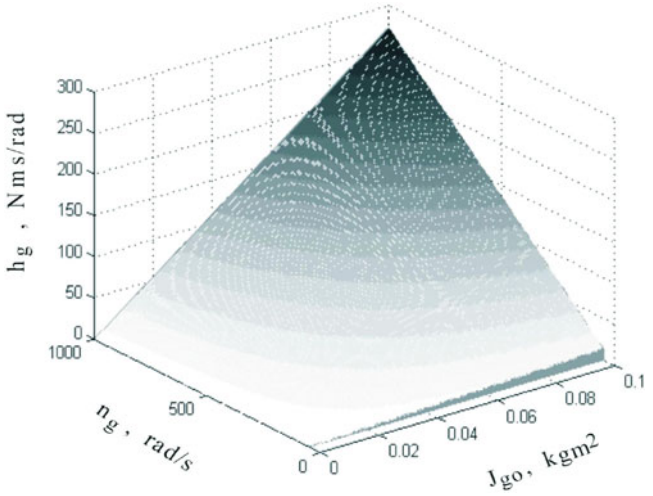

Fig. 4.30 Graph of mutual optimal relationships of damping coefficient of regulator h_g, angular velocity n_g, and moment of inertia I_{go}

From (4.129) we obtain the following value of the damping coefficient:

$$\bar{h}_g = \sqrt{2 + 4\bar{k}_b}. \tag{4.133}$$

Substituting (4.133) into (4.130) we obtain

$$\bar{k}_c = \frac{1}{2}\sqrt{2 + 4\bar{k}_b}. \tag{4.134}$$

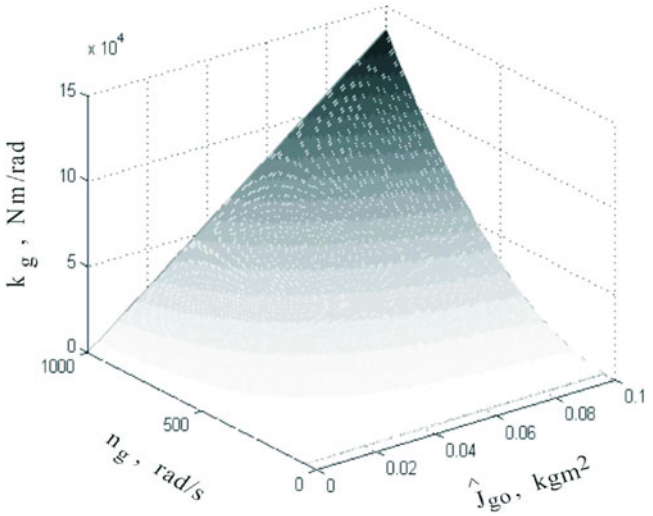

Fig. 4.31 Graph of mutual optimal relationships of gain coefficient of regulator k_g, angular velocity n_g, and moment of inertia I_{go}

Taking into account (4.125) we have

$$h_g = \sqrt{2I_{go}^2 n_g^2 + 4I_{gk}k_b}, \tag{4.135}$$

$$k_c = \frac{1}{2}\sqrt{2I_{go}^2 n_g^2 + 4I_{gk}k_b} \cdot \frac{I_{go}^2 n_g^2}{I_{gk}}. \tag{4.136}$$

Thus, the coefficients $\bar{h}_g$ and $\bar{k}_c$ are uniquely determined as functions of the gyroscope parameters I_{go}, I_{gk}, n_g and the coefficient $\bar{k}_b$, which should satisfy the stability conditions, and technical constraints resulting from the strength of the gyroscope.

The obtained relationships can be used to gyroscope control under conditions of alternating angular velocity of eigenrotations (e.g., in some self-guided missiles or target-seeking systems with a wide range of angular deviations of the gyroscope axis). Then one needs to measure simultaneously $n_g(t)$ and update the values of the regulator coefficients h_g and k_c according to the relationships (4.135) and (4.136). The coefficient k_b is given in a programmable way and it allows for adaptive control of the gyroscope.

Figures 4.27–4.31 graphically present the character of the relationships between particular gyroscope parameters. In order to obtain these relationships, one assumed that

$$I_{gk} = I_{go}/2.$$

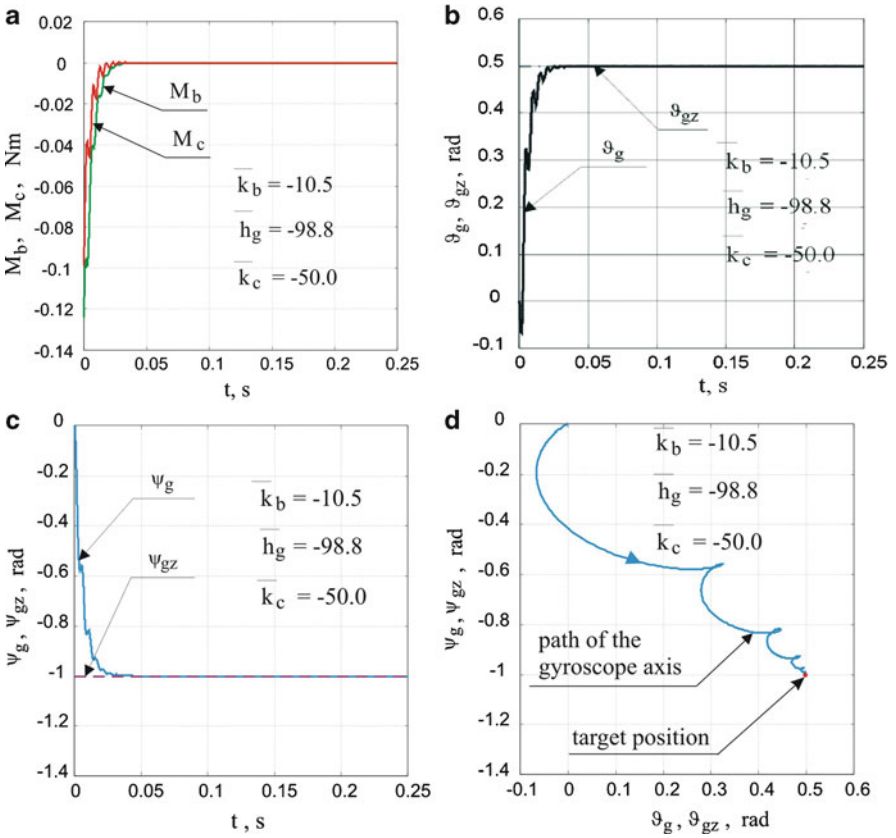

Fig. 4.32 Results of gyroscope axis control using optimal regulator during tracking of fixed point: (**a**) change of control torques as a function of time, (**b, c**) change in angular deviations as a function of time, (**d**) path of gyroscope axis

Thus, if the system of conditions (4.128)–(4.133) is satisfied, then the transient process of the gyroscopic system (4.121) will be damped during the shortest time [22]. Figures 4.32 and 4.33 present the results of gyroscope axis control upon tracking of a movable and fixed target using an optimal regulator of the coefficients determined from relationships (4.135) and (4.136).

In comparison with the results presented in Figs. 4.12–4.16 we can observe a significant improvement in the control quality of the gyroscope axis, i.e., considerable reduction of the duration of the transient process.

A gyroscope is a strongly non-linear system, which implies that errors of the preset and performed motion are generated at large values of angular velocities and deviations of the gyroscope axis. Therefore, when we apply program control within the non-linear range and under the influence of disturbance of gyroscope operation, it should also apply additional optimal control in a closed system.

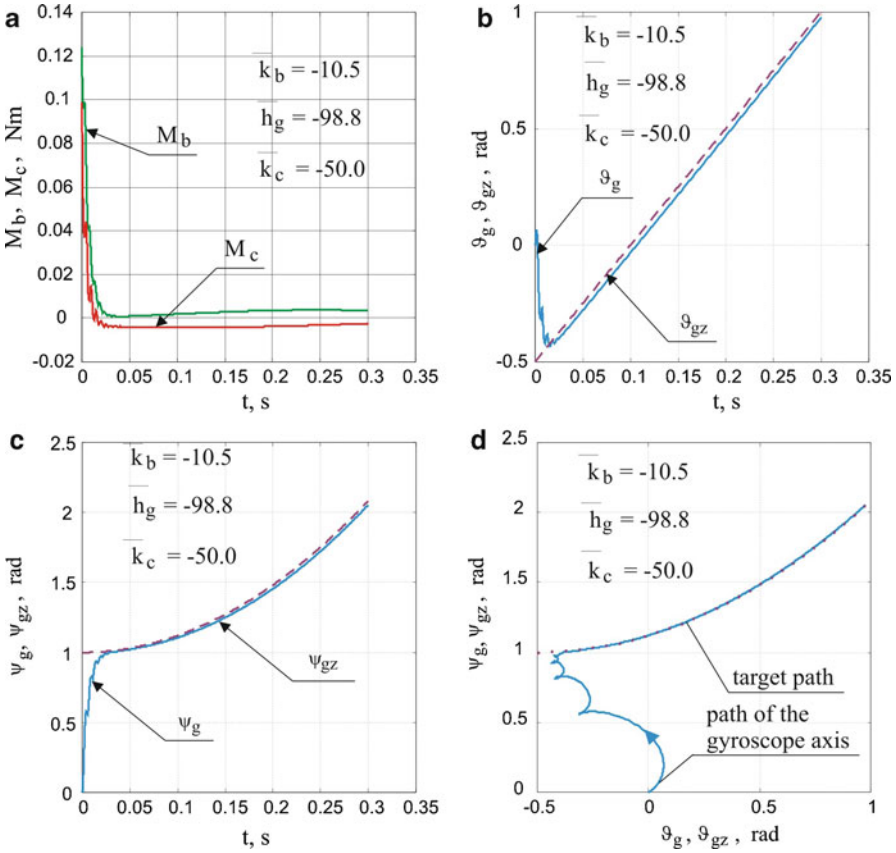

Fig. 4.33 Results of gyroscope axis control using optimal regulator during tracking of moving point: (**a**) change in control torques as a function of time, (**b, c**) change in angular deviations as a function of time, (**d**) path of gyroscope axis

References

1. Z. Koruba, in *Dynamics and control model of gyroscope located on deck of unmanned aerial vehicle.* North Atlantic Treaty Organization Unmanned Vehicles for Aerial, Ground and Naval Military Operations: A Symposium organized by the Applied Vehicle Technology Panel, Ankara, Turkey, 9–13 October 2000
2. J. Nizio, Dynamics of gyroscopes with a special emphasis on integrating gyroscopes in deterministic and probabilistic nonlinear formulations. *Mechanics* (Cracow University of Technology Press, Cracow, 1975), in Polish
3. V.A. Pavlov, *Aviational Gyroscopic Devices* (GOSIZDAT of Defense Industry, Moscow, 1954), in Russian
4. R. Grammel, *The Gyroscope: Its Theory and Applications* (Springer, Berlin, 1950), in German
5. M.A. Pavlovskiy, *Theory of the Gyroscopes* (Vyshaya Shkola, Kiev, 1986), in Russian
6. R.N. Arnold, L. Maunder, *Gyrodynamics and Its Engineering Applications* (Academic, New York, 1961)

7. K. Magnus, *Gyroscopes, Theory and Applications* (Springer, Berlin, 1971), in German
8. N.F. Babaeva, *Gyroscopes* (Mashinostroenie, Leningrad, 1973), in Russian
9. M. Davidson, *The Gyroscope and Its Application* (Hutchinson's Scientific and Technical Publications, London, New York, 1946)
10. R.F. Deimel, *Mechanics of the Gyroscope: The Dynamics of Rotation* (Dover, New York, 1950)
11. L.I. Kargu, *Measurement Devices of Flying Objects* (Mashinostroenie, Moscow, 1988), in Russian
12. J.W. Osiecki, A. Zgoa, in *Gyroscope axis movement control in nonlinear aspect.* Proceedings of the 1st National Conference on Avionics BIESZCZADY'95. Rzeszow-Jawor, vol. 1, no. (45) (Rzeszow University of Technology Scientific Papers Press, Avionics, Rzeszow, 1995), pp. 299–307, in Polish
13. Z. Koruba, Algorithm of direct gyroscope stabilizer control and correction. Int. J. Eng. Modell. **17**(1–2), 21–32 (2004)
14. L.I. Kargu, *Gyroscopic Devices and Systems* (Sudostroyeniye, Leningrad, 1988), in Russian
15. A.A. Odintsov, *Theory and Computation of Gyroscopic Systems* (Vyshaya Shkola, Kiev, 1985), in Russian
16. Z. Koruba, in *Dynamics of a gyroscope under control and its axis stabilization.* Proceedings of the 2nd School on "Methods for Active Vibration and Noise Reduction." Cracow–Zakopane, 26–28 April 1995, pp. 1955–1960
17. C.W. de Silva, *Mechatronics: A Foundation Course* (University of British Columbia, Vancouver, 2010)
18. Z. Koruba, A process of gyroscope motion control in an autonomous system, target detection and tracking. J. Theor. Appl. Mech. **37**(4), 908–927 (1999)
19. V.N. Koshlyakov, *Problems of Solid Body Dynamics and Applied Theory of Gyroscopes* (Nauka, Moscow, 1985), in Russian
20. M. Fusik, Z. Koruba, in *Model of a scanning device in a unmanned flying object.* Proceedings of the 7th Polish Conference on Automation and Exploitation of Control Systems, Gdynia, 13–15 October 1999, pp. 165–170, in Polish
21. Z. Koruba, J. Osiecki, *Construction, Dynamics and Navigation of Close-Range Missiles, Part 1*. University Course Book No. 348 (Kielce University of Technology Publishing House, Kielce, 1999), in Polish
22. Z. Koruba, Selection of the optimum parameters of the gyroscope system on elastic suspension in the homing missile system. J. Tech. Phys. **40**(3), 341–354 (1999), Warsaw, in Polish
23. R.B. Guenther, *An Introduction to Numerical Methods: A MATLAB Approach* (Oregon State University, Corvallis, 2005)
24. W.Bober, *Numerical and Analytical Methods with MATLAB* (Florida Atlantic University, Boca Raton, 2009)
25. S. Dubiel, Linear mechanical systems with the fastest damping. Theor. Appl. Mech. **3**(24), 15–28, (1986), Warsaw, in Polish